# Characterization and Functionality of Cardiac Progenitor Cells in Congenital Heart Patients

Rachana Mishra, PhD*; Kalpana Vijayan, PhD*; Evan J. Colletti, PhD; Daniel A. Harrington, PhD; Thomas S. Matthiesen, BS; David Simpson, PhD; Saik Kia Goh, BS; Brandon L. Walker, MS; Graça Almeida-Porada, MD, PhD; Deli Wang, MD, PhD; Carl L. Backer, MD; Samuel C. Dudley, Jr, MD; Loren E. Wold, PhD; Sunjay Kaushal, MD, PhD

***Background***—Human cardiac progenitor cells (hCPCs) may promote myocardial regeneration in adult ischemic myocardium. The regenerative capacity of hCPCs in young patients with nonischemic congenital heart defects for potential use in congenital heart defect repair warrants exploration.

***Methods and Results***—Human right atrial specimens were obtained during routine congenital cardiac surgery across 3 groups: neonates (age, <30 days), infants (age, 1 month to 2 years), and children (age, >2 to ≤13 years). C-kit$^+$ hCPCs were 3-fold higher in neonates than in children >2 years of age. hCPC proliferation was greatest during the neonatal period as evidenced by c-kit$^+$ Ki67$^+$ expression but decreased with age. hCPC differentiation capacity was also greatest in neonatal right atrium as evidenced by c-kit$^+$, NKX2–5$^+$, NOTCH1$^+$, and NUMB$^+$ expression. Despite the age-dependent decline in resident hCPCs, we isolated and expanded right atrium–derived CPCs from all patients (n=103) across all ages and diagnoses using the cardiosphere method. Intact cardiospheres contained a mix of heart-derived cell subpopulations that included cardiac progenitor cells expressing c-kit$^+$, Islet-1, and supporting cells. The number of c-kit$^+$–expressing cells was highest in human cardiosphere-derived cells (hCDCs) grown from neonatal and infant right atrium. Furthermore, hCDCs could differentiate into diverse cardiovascular lineages by in vitro differentiation assays. Transplanted hCDCs promoted greater myocardial regeneration and functional improvement in infarcted myocardium than transplanted cardiac fibroblasts.

***Conclusions***—Resident hCPCs are most abundant in the neonatal period and rapidly decrease over time. hCDCs can be reproducibly isolated and expanded from young human myocardial samples regardless of age or diagnosis. hCPCs are functional and have potential in congenital cardiac repair. **(*Circulation*. 2011;123:364-373.)**

**Key Words:** heart defects, congenital ■ cardiomyopathy ■ heart failure ■ remodeling ■ pediatrics ■ stem cells

The exact prevalence of pediatric heart failure is largely unknown but is growing because new treatments have increased the life expectancy of these patients. The number of congenital heart patients living presently outnumbers new congenital cardiac diagnoses, occurring in 35 000 to 40 000 infants per year in the United States.[1] Whereas adult heart failure is often ischemic in origin, the origin of pediatric heart failure is more varied, including a spectrum of cardiomyopathies, congenital heart defects (CHDs), and arrhythmias.[2] A novel emerging treatment for pediatric heart failure is cellular cardiomyoplasty whereby stem cells are delivered to the dysfunctional myocardium, an approach attempted thus far only in adults.[3–6]

**Clinical Perspective on p 373**

Most human studies have addressed the adult diseased myocardium, which is confounded by the presence of ischemia.[6–10] Despite significant progress in repair of the adult ischemic myocardium, the regenerative capabilities of human cardiac progenitor cells (hCPCs) have not been adequately explored in the nondiseased young human myocardium. Several issues regarding resident hCPCs in nondiseased young human myocardium need to be addressed. First, examination of age-related changes in the hCPC profile of young postnatal nondiseased myocardium is needed. Second, identification of the best anatomic source of hCPCs within the heart is required. Finally, a reproducible method for the

Received March 11, 2010; accepted November 15, 2010.

From the Division of Cardiovascular-Thoracic Surgery, Children's Memorial Hospital, Chicago, IL (R.M., K.V., D.A.H., T.S.M., D.S., S.K.G., B.L.W., D.W., C.L.B., S.K.); Northwestern University Feinberg School of Medicine, Chicago, IL (C.L.B., S.K.); Department of Animal Biotechnology, University of Nevada, Reno (E.J.C., G.A.-P), Division of Cardiology, Department of Medicine, University of Illinois at Chicago, Chicago (S.C.D.); and Center for Cardiovascular and Pulmonary Research, The Research Institute at Nationwide Children's Hospital, The Ohio State University, Columbus, OH (L.E.W.).

*Drs Mishra and Vijayan contributed equally to this article.

**The online-only Data Supplement is available with this article at http://circ.ahajournals.org/cgi/content/full/CIRCULATIONAHA.110.971622/DC1.**

Correspondence to Dr Sunjay Kaushal, Children's Memorial Hospital, Division of Cardiovascular-Thoracic Surgery, 2300 Children's Plaza, mc 22, Chicago, IL 60614. E-mail skaushal@childrensmemorial.org



*Circulation* **is available at http://circ.ahajournals.org** **DOI: 10.1161/CIRCULATIONAHA.110.971622**

generation and expansion of hCPCs from small surgical samples in vitro needs to be determined. We believe that congenital heart patients may be the ideal source to study these important questions because they have normal contracting myocardium with an anatomic structural abnormality.

Understanding the properties of hCPCs in young CHD patients offers important insight into the role of hCPCs in the maintenance of young maturing myocardium and their potential for use in novel congenital cardiac repair strategies. Here, we describe the resident hCPCs present in the human heart and how this population of cells changes with age in neonates (<30 days of age), infants (1 month to 2 years of age), and children (>2 to ≤13 years of age). We further isolated progenitor cells by the cardiosphere technique[6] and used human cardiosphere-derived cells (hCDCs) for cardiac differentiation studies. hCDCs are a mixed cell population containing hCPCs and supporting cells and are already in an adult clinical trial (Cardiosphere-Derived Autologous Stem Cells to Reverse Ventricular Dysfunction [CADUCEUS; NCT00893360] and Autologous Human Cardiac-Derived Stem Cell to Treat Ischemic Cardiomyopathy [ALCADIA; NCT00981006]; http://clinicaltrials.gov) for cardiac regeneration. Finally, we tested the functionality of hCDCs and their ability to differentiate into cardiac lineages in vivo in a rat model of myocardial infarction.

## Methods

An expanded Methods section for tissue processing and immunostaining is available in the online-only Data Supplement.

### Tissue Samples

This study was approved by the Institutional Review Committee at Children's Memorial Hospital. After parental consent was given, specimens (70±80 mg; mean, 40 mg) from the right atrial (RA) appendage were obtained from young patients (n=118) during routine congenital cardiac surgeries and specimens (n=3) from all chambers of the explanted cardiomyopathic hearts after cardiac transplantation. Fifteen tissue samples were processed for immunostaining and 103 tissue samples were processed for harvesting hCPCs. As shown in Table I in the online-only Data Supplement, patients ranged in age from 1 day to 13 years with various cardiac diagnoses.

### Immunohistochemical Staining of RA Tissues

Specimens were fixed and processed through the use of standard methods. Cryostat sections (7 to 10 $\mu$m) were stained with primary antibodies as noted and secondary Alexa Fluor–conjugated antibodies. Immunostained sections were examined by confocal microscopy, and the number of labeled cells was determined as a percentage of the total DAPI-labeled nuclei.

### Generation of CDCs

hCDCs were generated through the use of the protocol described by Smith et al[6] with modifications. Briefly, RA tissue was minced and mildly digested with 0.05% trypsin/EDTA and collagenase type II (Worthington Biomedical Corp, Lakewood, NJ). Explants were plated on fibronectin in Iscove modified Dulbecco medium with 20% FBS. At 2 to 3 weeks after plating, phase-bright cells were removed and plated at low density (1.5 to $3\times10^4$ cells per 1 mL) in cardiosphere-growing medium (CGM). Cardiospheres were removed and plated on fibronectin in human cardiac stem cell expansion medium (HCSCEM; Celprogen, San Pedro, CA). Phase-bright cells were harvested from individual explant cultures every 3 to 5 days up to 4 consecutive times. hCDCs were then expanded on fibronectin-coated plates.

### Immunostaining of Cardiospheres and CDCs

Intact cardiospheres and hCDC monolayers were immunostained using standard methods with primary antibodies and fluorochrome-tagged secondary antibodies as noted in the online-only Data Supplement. After nuclear DAPI staining, cells were visualized with confocal microscopy.

### Flow Cytometry Analysis of CDCs

CDCs were passaged 4 times and then evaluated for flow cytometry experiments with a Becton-Dickinson FACS Calibur (San Jose, CA) with 10 000 events collected. Cells were incubated with fluorochrome-conjugated antibodies against c-kit, CD90, CD105, and a lineage cocktail (Lin1) of antibodies against hematopoietic lineage surface markers (CD3, CD14, CD16, CD19, CD20, and CD56).

### In Vitro Cardiac Lineage Differentiation Assays

Cell differentiation assays were performed as previously described.[10,11]

### Cell Transplantation and Echocardiography

Myocardial infarction was created in immunodeficient male nude rats by permanent ligation of the left anterior descending coronary artery as previously described.[12] For intracardiac grafting, the hCDCs were injected into the anterior infarct and peri-infarct regions.

### Regeneration Quantification

Masson trichrome–stained sections were taken from the midportion at the level of the midpapillary muscle of the infarcted myocardium as described.[6] Myocardial viability within the infarct zone was determined with Masson trichrome–stained sections by tracing the infarct borders. With the use of ImageJ software, the viable myocardium was then calculated within the overall infarcted zone by the number of red pixels (viable tissue) divided by overall number of pixels. Six sections per animal and 5 animals per group were analyzed.

### Statistical Analyses

Calculations of c-kit$^+$, NKX2–5$^+$, Ki67$^+$, NOTCH1$^+$, NUMB$^+$, and GATA-4$^+$ cells in RA sections were derived from 30 microscopic fields per tissue sample comprising 200 to 500 cells per field. Immunohistochemical data are representative for neonates (n=4), infants (n=6), and children >2 years of age (n=5). Flow cytometric analyses represent sample n values for the 3 age groups: neonates (n=5), infants (n=14), and children >2 years of age (n=7). A Poisson regression model was used to model rates of c-kit, NKX2–5, and Ki67 expression. Pair-wise comparisons among the 3 age groups were also conducted. A linear mixed model with a random intercept effect was applied to analyze ejection fraction and shortening fraction changes between the 3 groups over time. Contrasts between the 3 experimental groups at days 7 and 28 were conducted in the linear mixed model. All analyses were conducted with SAS 9.2.

## Results

### C-Kit Expression Declines With Age in RA

Because c-kit is a prominent marker for resident CPCs, we examined the occurrence of c-kit$^+$ cells within the 4 heart chambers. We hypothesized that there is an increased presence of c-kit$^+$ hCPCs in the atria compared with the ventricles because the decreased wall stress in atrial chambers would favor hCPC maintenance and proliferation.[13] Because it is difficult to obtain myocardial samples from all 4 heart chambers of a single congenital heart patient, we examined the presence of hCPCs in all 4 chambers of cardiomyopathic hearts excised for transplantation. Expression of c-kit was

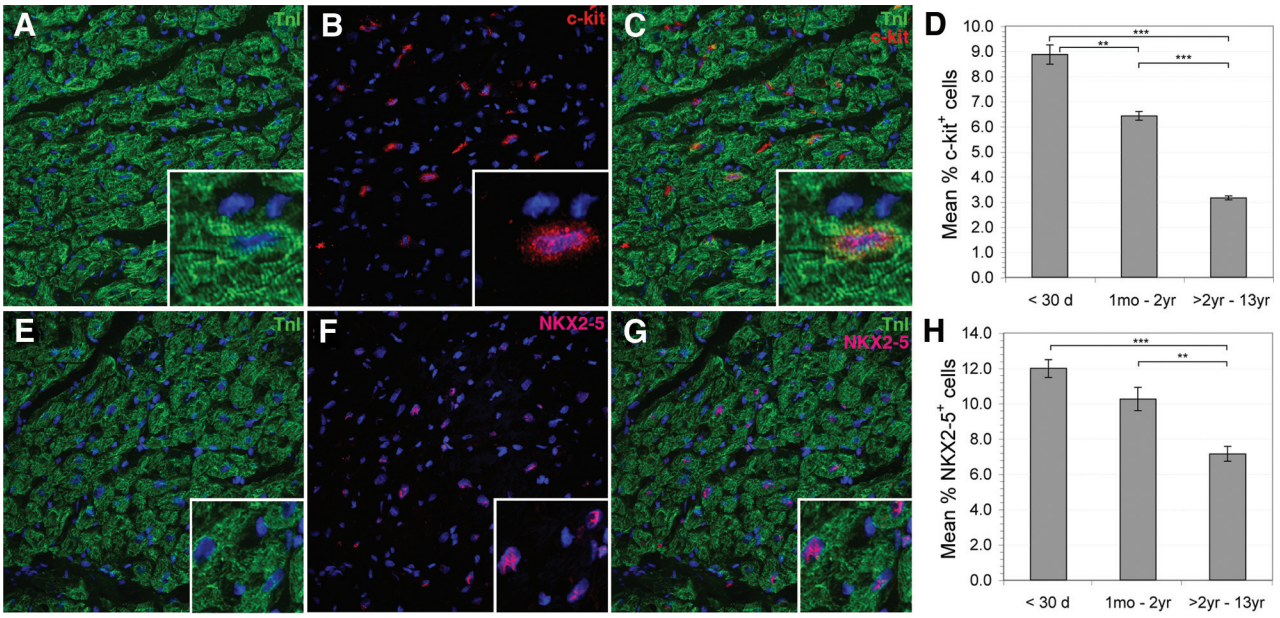


**Figure 1.** C-kit and NKX2–5 expression was greater in neonates and declined with age. Confocal microscopy images identify c-kit$^+$ (A through C) and NKX2–5$^+$ cells (E through G) in intact RA. Cardiac TnI with nuclear DAPI staining is shown (A and E). Serial staining for myocardial TnI (A and E), c-kit (B), and NKX2–5 (F) is shown with DAPI nuclear staining in blue. Merged images are shown (C and G) to illustrate colocalization with muscle bundles. The inserts show a magnified field. Graphs indicate the relative mean percentages of c-kit$^+$ (D) and NKX2–5$^+$ (H) cells across patient age groups (error bars are ±SEM). **$P<0.0001$, ***$P<0.0001$.

highest within the RA (5.2%) compared with the right ventricle (1.4%), left ventricle (1.4%), and left atrium (0.3%; $P<0.05$; Figure I in the online-only Data Supplement). Because of the high expression of c-kit$^+$ in the RA, we focused on the RA for further CPC analysis. In myocardial sections, c-kit$^+$ cells could be found among and closely opposed to TNI$^+$ cardiomyocytes (Figure 1C). C-kit expression was highest in neonates (8.9±0.4%) and declined with advancing age. Significantly lower percentages of c-kit$^+$ cells were observed in infants (6.4±0.2%; relative risk [RR], 1.38; 95% confidence interval [CI], 1.33 to 1.45; $P<0.0001$) and children >2 years of age (3.2±0.1%; RR, 2.50; 95% CI, 2.37 to 2.64; $P<0.0001$; Figure 1D). No difference in c-kit expression between cyanotic and noncyanotic patients was observed ($P>0.05$). Furthermore, costaining of the c-kit$^+$ cells with tryptase, a marker for mast cells within myocardial tissue, was infrequent (<0.5%; Figure II in the online-only Data Supplement).

## NKX2–5 Expression Declines With Age in RA

Cardiomyogenic commitment in CPCs is indicated by expression of cardiac-specific transcription factors such as NKX2–5 and GATA-4. During development, NKX2–5 and GATA-4 interact in a synergistic manner to promote cardiac transcription.[14] NKX2–5 expression by itself in RA sections is shown in Figure 1E through 1H. Cells expressing NKX2–5 were located within cardiac muscle fascicles, as evidenced by colocalization with troponin I (TnI; Figure 1G). NKX2–5 expression was highest in neonates (12.0±1.0%) compared with infants (10.3±1.0%; RR, 1.51; [95% CI, 1.46 to 1.58; $P<0.0001$) and children >2 years of age (7.2±0.4%; RR, 2.06; 95% CI, 1.99 to 2.14; $P<0.0001$; Figure 1H). NKX2–5 expression levels did not differ between cyanotic versus noncyanotic patients ($P>0.05$).

To identify hCPCs that were committed to a cardiomyogenic lineage, hCPCs coexpressing c-kit and NKX2–5 were examined (Figure 2A through 2D). Coexpression of c-kit and NKX2–5 was highest in neonates (2.9±0.1%) and declined significantly to 1.0±0.1% (RR, 2.90; 95% CI, 2.63 to 3.19; $P<0.0001$) in children who were >2 years of age (Figure 2D), indicating that the number of cardiomyogenic lineage-committed hCPCs also declined with age. No statistically significant difference in c-kit$^+$NKX2–5$^+$ CPCs between cyanotic and noncyanotic patients was observed.

## Decline in Identifiable CPC and Proliferation of CPC With Increasing Age

We examined the expression of Ki67, a marker for proliferating cells, in RA sections (Figure 2E through 2I). Ki67 expression was highest during the neonatal period and declined with advancing age (Figure 2E through 2H). Neonates exhibited 15.0±0.1% Ki67$^+$ cells; infants had 8.0±0.3% (RR, 1.52; 95% CI, 1.46 to 1.58; $P<0.0001$); and children >2 years of age had 5.0±0.2% (RR, 2.16; 95% CI, 2.07 to 2.26; $P<0.0001$). Proliferative hCPCs in RA were identified by c-kit and Ki67 coexpression. C-kit$^+$Ki67$^+$ cells were highest in neonates (5.4±0.2%). There was a statistically significant decline in expression with increasing age to 0.9±0.03% (RR, 5.60; 95% CI, 5.08 to 6.18; $P<0.0001$) in children >2 years of age (Figure 2H). We further investigated hCPC proliferation by examining the number of c-kit$^+$Ki67$^+$ cells as a fraction of the total number of c-kit$^+$ cells (Figure 2I). Interestingly, in neonates, 61.1±3.7% of c-kit$^+$ cells coexpressed Ki67. In contrast, only 28.1±1.5% and 29.2±1% of c-kit$^+$ cells coexpressed Ki67 in infants (RR, 2.9; 95% CI, 2.71 to 3.12; $P<0.0001$) and children >2 years of age (RR, 1.93; 95% CI, 1.73 to 2.14; $P<0.0001$). Thus, our

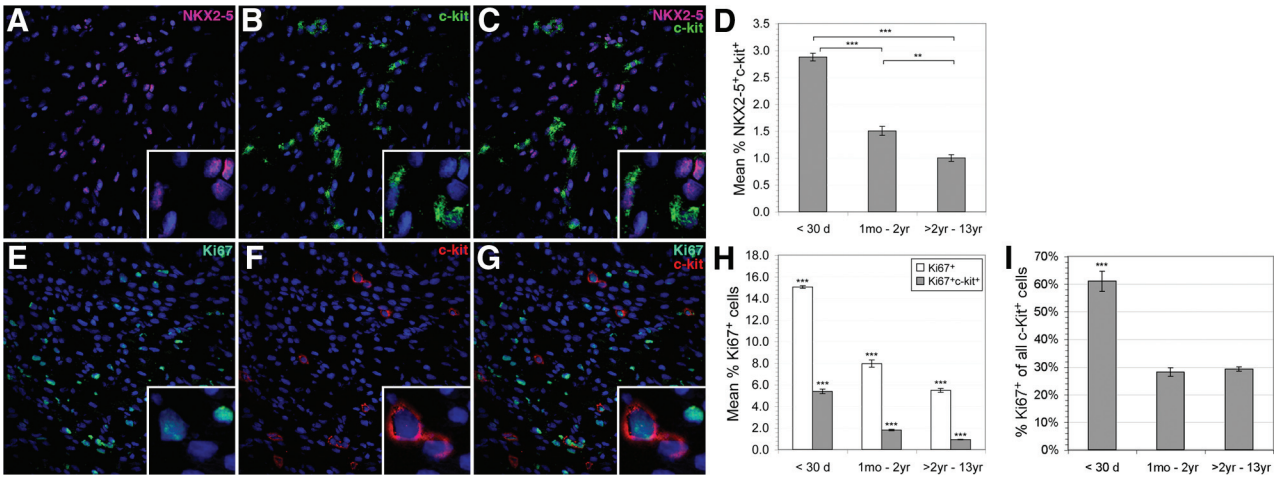


**Figure 2.** Confocal microscopy images identify c-kit$^+$NKX2–5$^+$ coexpression (A through C) and c-kit$^+$Ki67$^+$ coexpression (E through G) in intact RA. C-kit$^+$ and NKX2–5$^+$ expression is shown with nuclear DAPI staining in A and B, respectively. C, Merged image showing c-kit$^+$NKX2–5$^+$ coexpression. D, Graph illustrating age-related trends for c-kit$^+$NKX2–5$^+$ coexpression which was highest during the neonatal period (2.9±0.1%) and declined significantly with increasing age. C-kit$^+$ and Ki67$^+$ expression is shown with nuclear DAPI staining (blue; E and F) and merged c-kit$^+$Ki67$^+$ coexpression is displayed in G. H, Graph illustrating age-related trends for c-kit$^+$Ki67$^+$ coexpression. Total Ki67 expression and c-kit$^+$Ki67$^+$coexpression were highest in neonates (15.0±0.1% and 5.4±0.2%, respectively) and significantly declined with age. I, C-kit$^+$Ki67$^+$ cells as a fraction of the total c-kit$^+$ cells. In neonates, c-kit$^+$Ki67$^+$ cells represented 61.1±3.7% of total c-kit$^+$ cells. Infants and children >2 years of age had 28.1±1.5% and 29.2±1%, respectively. Error bars are ±SEM. ***P*<0.0001, ****P*<0.0001.

results indicated a marked (≈50%) decline in the number of proliferating hCPCs with increasing age. No statistically significant difference was observed in c-kit$^+$Ki67$^+$ coexpression between cyanotic and noncyanotic patients ($P>0.05$).

## NUMB Declines but GATA-4 Expression Remains Unchanged With Age in the RA

Signaling via NOTCH receptors maintains stem cell populations and promotes progenitor cell proliferation. NUMB inhibits NOTCH signaling via direct interaction with NOTCH receptors, preventing their nuclear translocation.[15] The impact of NOTCH/NUMB signaling has not been examined in young human myocardium. We therefore examined NUMB expression in resident hCPCs and determined that NUMB-expressing cells were greatest in neonatal tissue and that these cells frequently coexpressed c-kit and Ki67 (Figure 3A to 3B). The expression of NUMB in neonatal RA was 1.2±0.42% and disappeared in patients who were >2 years of age (Figure 3C). Approximately 50% of NUMB-expressing cells coexpressed GATA-4 (Figure 3E). Examination of GATA-4 and Ki67 coexpression revealed that ≈5% of cells expressed both markers in neonates with a subsequent decline in expression in older age groups (Figure 3D). There was no statistically significant change in total GATA-4 expression with age, ranging from 11.25±0.78% in neonates to 12.75±0.86% in children >2 years of age (Figure 3F). NOTCH1 was expressed in the heart tissues in all 3 age groups at a level of ≈20%; however, activated NOTCH1 expression was detected only in neonates (1.3%), not in older age groups (Figure 3G).

## Generation of hCDCs From RA Tissue Specimens

Progenitor cells were isolated and expanded from RA explant cultures with the use of a modified version of the cardiosphere method[6] (Figure 4). RA specimens ranging from 25 to 315 mg were mildly digested and plated as explants on fibronectin. Explants adhered to fibronectin-coated surfaces 1 week after plating (Figure 4A). Between 1 and 2 weeks, a monolayer of fibroblast-like cells grew around individual explants (Figure 4B). At approximately 2 to 3 weeks after plating, phase-bright cells would appear, migrating over the fibroblast-like monolayer (Figure 4C). Phase-bright cells were removed by mild trypsinization and plated at a low density in cardiosphere-growing medium to form cardiospheres (Figure 4D). Phase-bright cells were harvested every 3 to 5 days up to 4 times from individual explant cultures. Cardiospheres were removed and replated in HCSCEM for expansion of hCDCs (Figure 4E). Immunostaining of intact cardiospheres identified cells that expressed c-kit, NKX2–5, GATA-4, Islet-1 (ISL1), and TnI (Figure 4F through 4J). C-kit$^+$ cells were located both on the outer surface and within the cardiosphere core. Extensive expression of NKX2–5 was observed throughout the cardiosphere; however, GATA- 4 expression was limited to cells on the outer surface. ISL1-expressing cells were visible both on the outer surface and within the cardiosphere core. Cells expressing the cardiac myofilament protein TnI occurred in isolated clusters on the outer surface and within the cardiosphere core.

## Expansion of hCDC Monolayers

hCDC monolayers could be expanded up to 20 to 30 days after initial plating in HCSCEM (Figure III in the online-only Data Supplement). Cell yield was ≈156 000±54 000 cells per 1 mg tissue, with yields upward of $2\times10^6$ cells generated from RA specimens with a starting weight of ≥40 mg, usually obtained from infants and children >2 years of age. Neonatal RA specimens had starting weights ranging from 8 to 30 mg and did not generate such high cell yields. Growth rates of hCDCs were variable between different harvest generations of hCDCs from individual explant cultures derived from different patient specimens (Figure IIIA in the

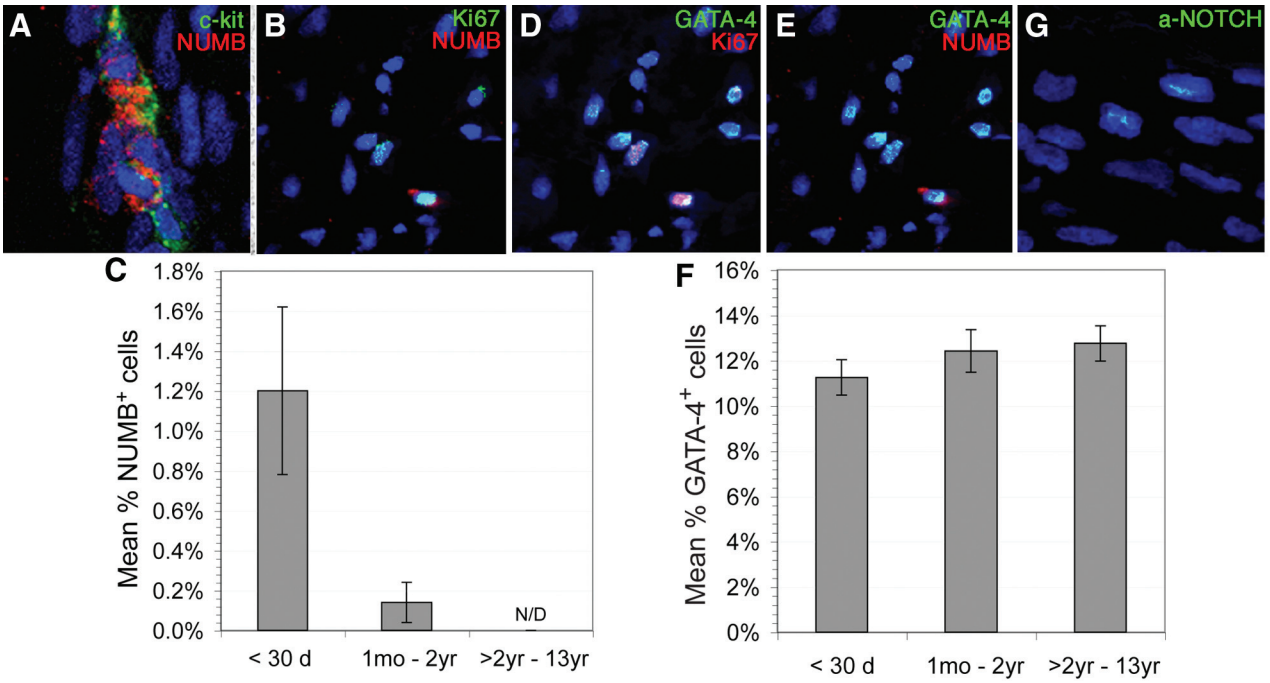


**Figure 3.** Confocal microscopy images demonstrate NUMB and GATA-4 expression and coexpression with c-kit and Ki67 in intact neonatal RA with nuclear DAPI staining (blue). Graphs indicate age-related trends for NUMB and GATA-4 expression (C and F). NUMB expression was low in neonatal RA (1.2±0.42%) and declined with age, being undetectable in patients >2 years of age (C). GATA-4 expression did not differ among neonates (11.25±0.78%), infants (12.42±0.94%), and children >2 years of age (12.75±0.86%) (F). Error bars are ±SEM. Activated NOTCH1 was detected in neonates (1.3%) but was absent in older groups (G).

online-only Data Supplement). Growth rates of hCDCs derived from either the second- (Figure IIIB in the online-only Data Supplement) or third- (Figure IIIC in the online-only Data Supplement) harvest generations from RA specimens across patients of different ages were also variable. hCDCs could be expanded beyond 10 passages in HCSCEM, still maintaining their previous biochemical markers.

## hCDCs at Early Passage Express NKX2–5

To determine whether expanded hCDCs remained in an uncommitted state or underwent cardiac lineage commitment, hCDCs at early passage were examined for expression of early embryonic and postlineage commitment markers (Figure IV in the online-only Data Supplement). hCDCs were examined by confocal microscopy at early passage (P0) ≈6 to 7 days after initial plating in CSCEM for embryonic stem cell markers SSEA-4 and Oct3/4 (Figure IVA and IVB in the online-only Data Supplement), as well as c-kit and the cardiac lineage transcription factor NKX 2.5 (Figure IVC and IVD in the online-only Data Supplement). Expression of the embryonic stem cell markers Oct3/4 and SSEA-4 was extremely rare (<1%). C-kit$^+$ cells were detected at P0 (≤5%; Figure

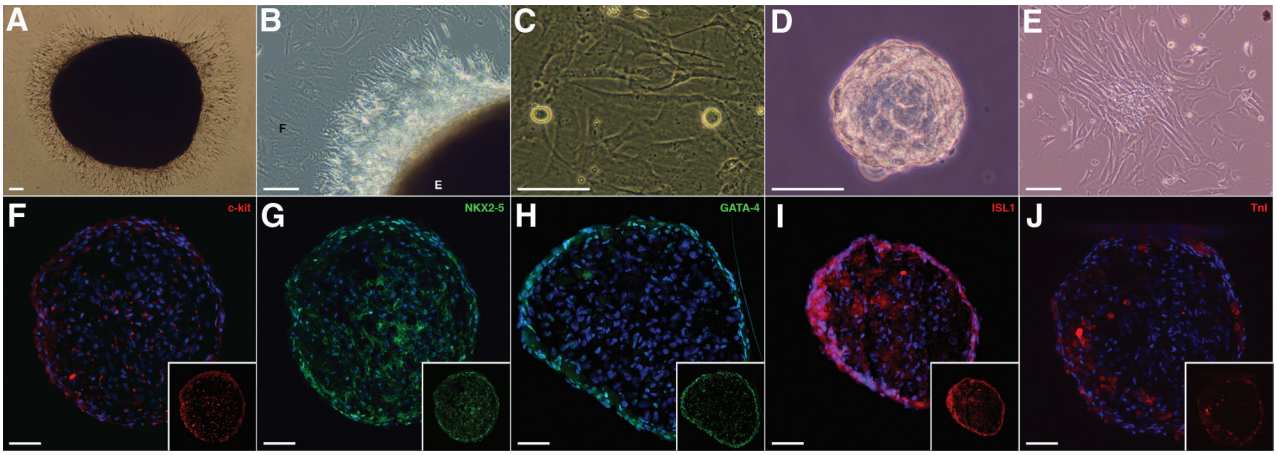


**Figure 4.** A through E, The generation of hCDCs from RA explant cultures. A, Image showing an adherent explant at 1 week after plating. The edge of an adherent tissue explant (B) and surrounding fibroblast-like monolayer (C) are shown. Phase-bright cells migrating above the fibroblast-like monolayer are indicated. D, Removal and replating of phase-bright cells in cardiosphere-growing medium–induced cardiosphere formation. Cardiospheres were replated in HCSCEM to expand hCDC monolayers (E). Intact cardiospheres were sectioned and stained for c-kit (F), NKX2–5 (G), GATA-4 (H), ISL1(I), and TnI (J). Nuclei were identified by DAPI staining (blue). Scale bar=50 μm.

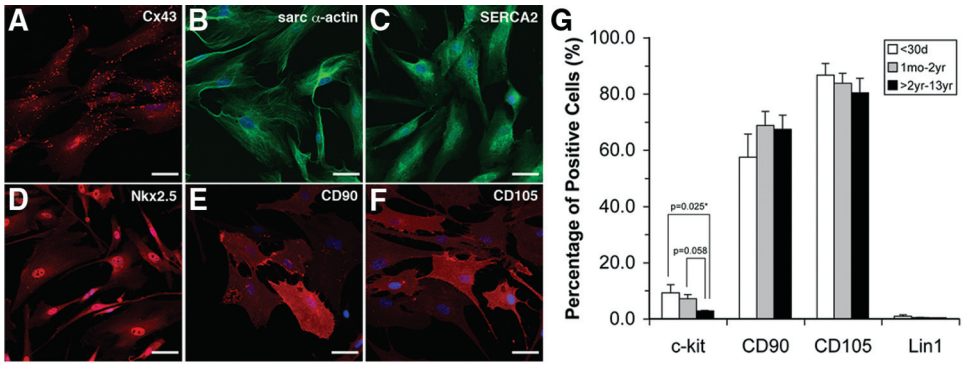


**Figure 5.** Confocal microscopy images of CDC at late passage (P4) are shown. A through C, Expression of cardiomyocyte-specific markers. A, Clusters of CDCs expressed connexin 43 (Cx43). The majority of CDC expressed α-sarcomeric actin (α-actin) and SERCA2 (B and C). CDCs at P4 also expressed NKX2–5 (D) and mesenchymal markers CD90 and CD105 (E and F). Flow cytometry analysis of CDC at P4 (G). CDCs were negative for hematopoietic lineage (Lin1) and positive for CD90 (65±5%) and CD105 (81±3%). C-kit$^+$ CDCs were higher in neonates (9±3%) and infants (7±2%) compared with children >2 years of age (3±0.3%). Coexpression of c-kit with CD90 and CD105 was observed (45% to 64%) in the majority of patient samples with no difference between patient age groups. Error bars are ±SEM.

IVC in the online-only Data Supplement), and the majority of cells (95%), regardless of patient age, expressed NKX2–5 (Figure IVD in the online-only Data Supplement). Furthermore, hCDCs were negative for collagen type I, a fibroblast marker (Figure V in the online-only Data Supplement).

## hCDCs at Late Passage Express Cardiomyocyte Markers

Because the majority of hCDCs at P0 expressed NKX2–5, indicating cardiomyogenic lineage, we examined whether hCDCs at late passage (P4) expressed cardiomyocyte markers (Figure 5). Clusters of hCDCs expressed connexin 43, whereas the majority of hCDCs expressed α-sarcomeric actin, sarcoplasmic reticulum $Ca^{2+}$ ATPase (SERCA2), and NKX2–5 (Figure 5A through 5D). Expression of mesenchymal markers CD90 and CD105 was also observed (Figure 5E and 5F).

## hCDCs at Late Passage Express C-Kit And Mesenchymal Markers

Earlier studies report that hCDCs exhibit a mesenchymal phenotype expressing CD90 and CD105.[6,16,17] Flow cytometric analysis of hCDCs at P4 (Figure 5G) showed that our hCDCs were predominantly negative for hematopoietic lineage (Lin1) markers (CD3, CD14, CD16, CD19, CD20, and CD56). A substantial number of cells expressed CD90 and CD105. The relative percentages of CD90$^+$ and CD105$^+$ hCDCs did not differ significantly between age groups. The percentage of c-kit$^+$ cells was higher in neonates (9±3%) and infants (7±1%) compared with children >2 years of age (3±0.3%). A significant proportion of c-kit$^+$ cells coexpressed CD90 or CD105 (45% to 64%). The relative percentage of c-kit$^+$CD90$^+$ and c-kit$^+$CD105$^+$ hCDCs did not differ significantly between patient groups. The percentage of c-kit$^+$ cells did not differ between hCDC populations derived from cyanotic and noncyanotic patients. This trend was also true for CD90 and CD105 expression. The idea of CD90$^+$ and CD105$^+$ cells being support cells for the c-kit$^+$ population has been proposed,[6,16] suggesting that hCDCs with higher CD90$^+$ or CD105$^+$ expression levels should have correspondingly higher c-kit expression. However, we found no such correlation between either CD90 or CD105 and c-kit expression.

## Functionality and Cardiac Multilineage Ability of hCDCs

To investigate the differentiation potential of the hCDCs into multiple cardiovascular lineages, 2 sets of experiments were performed. First, we differentiated hCDCs into the 3 different cardiac lineages with specific selected medias. The hCDCs were plated and then further differentiated with lineage-specific media for 14 days as previously described.[10,11] Immunohistochemical analysis showed that the hCDCs differentiated into 3 different cardiac lineages (Figure 6A through 6C) at roughly 1% efficiency, which was determined by TnI staining for cardiomyocytes, by smooth muscle actin staining for smooth muscle cells, and by PECAM-1 staining for endothelial cells. No statistically significant difference in the in vitro differentiation efficiency was seen among the hCDCs derived from patients of different ages. These results indicated the cardiac multilineage potential of the hCDCs in vitro that may contribute to their eventual functionality in vivo.

The second experiment involved a randomized blinded study to evaluate the effectiveness of the hCPCs to rescue the infarcted myocardium of immunodeficient rats. Shortly after ligation of the left anterior descending artery in immunodeficient rats, hCDCs or human cardiac fibroblasts were injected into the ventricular wall of the peri-infarct and infarct regions. In addition, the same amount of media was used as control. The functionality of the hCDCs within the infarcted myocardium was examined by echocardiography, and engraftment of the hCDCs was assessed by histological analysis.

To evaluate the cardiac function, echocardiography was performed before and at 7 and 28 days after left anterior descending ligation. At baseline, left ventricular ejection fraction and fractional shortening were similar among all rats receiving hCDCs, cardiac fibroblasts, or control (Figure 7A and 7B). Echocardiography performed at 28 days revealed a higher left ventricular ejection fraction (41.5±3.3%) and fractional shortening (18.0±1.6%) in hearts receiving hCDCs

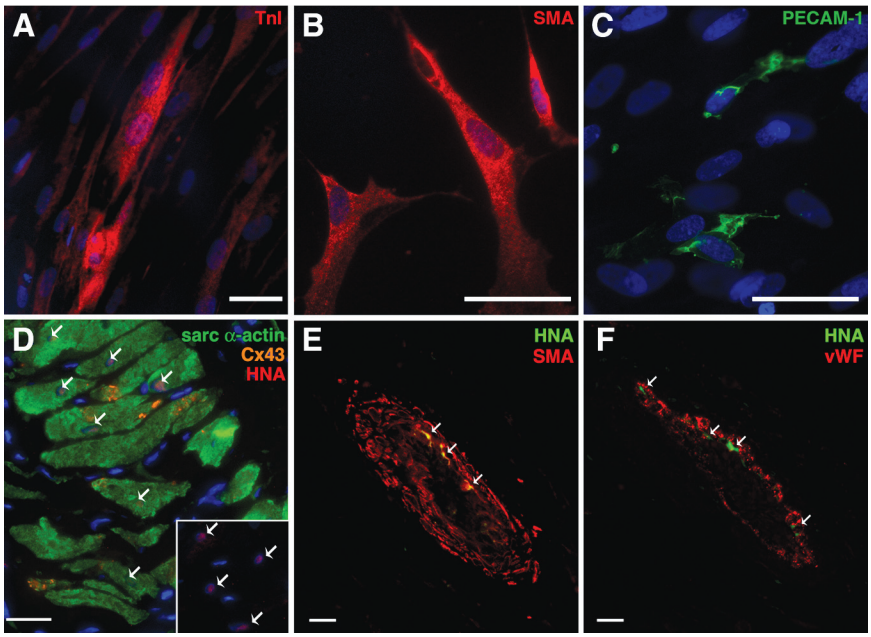


**Figure 6.** Differentiation of the hCDCs in vitro and in vivo into cardiac lineages. In vitro assays for 14 days determined the cardiac lineage potential by differentiating toward myogenic, endothelial, and smooth muscle lineages (A through C). Cardiomyogenic differentiation of the hCDCs was confirmed by positive staining for cardiac TnI(A). Smooth muscle and endothelial differentiation as confirmed by α-smooth muscle actin (B) and PECAM (C) staining, respectively. hCDCs were injected into the infarcted myocardium of the rat, and histological analysis was performed at 28 days (D through F). Transplanted hCDCs were tracked by their expression of human nuclear antigen protein (HNA; red) and colocalization with sarcomeric α-actin (green) and gap junction protein connexin 43 (Cx43; orange; D). Inset, The tracked HNA protein (red; marked with arrows). The transplanted hCDCs differentiated into smooth muscle cells, which colocalized with α-smooth muscle actin (SMA; red; E) and into endothelial cells, which colocalized with von Willebrand factor (vWF; red; F). Nuclei are stained blue with DAPI.

than in those receiving cardiac fibroblasts or control (left ventricular ejection fraction, 30±3.2%, $P=0.01$ for cardiac fibroblasts; 30±1.6%, $P=0.004$ for control and fractional shortening; 14.7±0.1%, $P=0.01$ for cardiac fibroblast; and 12.7±1.8%, $P=0.009$ for control). There was no difference among cardiac fibroblasts or control media–treated hearts ($P=0.3$). Furthermore, there was no difference in functional recovery among the hCDCs derived from patients of different ages. The improved left ventricular ejection fraction and fractional shortening in the hCDC-treated hearts were maintained from day 7 to 28 and represented the sustained effect of the hCDCs. Together, these data indicate that hCDC transplantation results in enhanced functional recovery and more favorable remodeling in the infarcted myocardium.

We further examined the impact of hCDCs on the pathological features of the infarcted myocardium by examining myocardial histology 28 days after transplantation. By tracking the hCDCs with a human nuclear marker, we observed numerous hCDCs in the peri-infarct and infarct regions (Figure 6D). Immunophenotypic characterization revealed that the engrafted hCDCs stained positive for the cardiac sarcomeric α-actin. The hCDCs formed a mass of engrafted myocardium that appeared morphologically similar to mature cardiomyocytes and was indistinguishable from other cardiomyocytes in that region. Furthermore, hCDC-derived cardiomyocytes formed gap junctions with the native cardiomyocytes as demonstrated by connexin 43 expression (Figure 6D). Phenotypic changes of hCDCs into smooth cells and endothelial muscle cells were also confirmed by the colocalization of transplanted hCDCs with von Willebrand factor and α-smooth muscle actin (Figure 6E and 6F). In contrast, we did not detect differentiation of the transplanted cardiac fibroblasts into cardiomyocytes, smooth muscle cells, or endothelial cells. Cardiomyogenic differentiation, as defined by sarcomeric protein expression and the morphological similarity to native myocardium, was observed in all immunodeficient rats transplanted with hCDCs. An organized mass of regenerative hCDC- derived tissue, similar to normal host myocardium (Figure 6D), was detected in hearts from 4 of 5 rats (80%), and only scattered cellular differentiation was observed in the 1 remaining rat (20%). Despite this, all hCDC-transplanted rats had hCDC-specific protein expression, including cardiomyocytes, smooth muscle cells, and endothelial cells (Figure 6D through 6F).

Regeneration was further quantified in sections stained with Masson trichrome to discern viable tissue from fibrous tissue. A typical Masson staining pattern in hearts transplanted with hCDCs is shown in Figure 8A. Positive red-

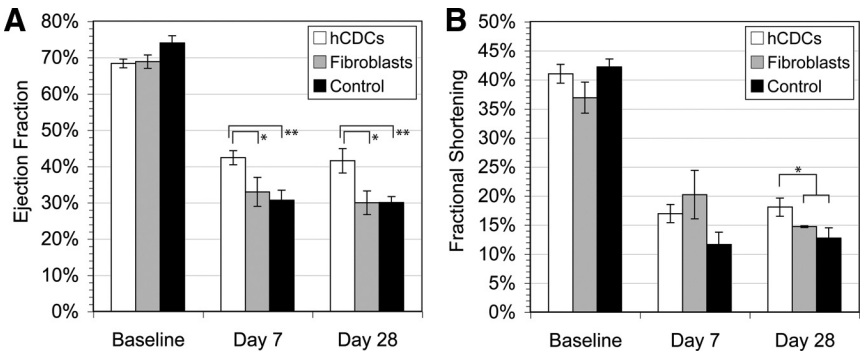


**Figure 7.** A and B, Functional improvement after myocardial infarction in transplanted rat hearts. Left ventricular ejection fraction (EF) and fractional shortening were analyzed by echocardiography for all 3 experimental groups in triplicate recordings: hCDCs (n=6), cardiac fibroblasts (n=4), and control (n=5). A, At 7 days, *$P=0.08$ and **$P=0.001$ relative to the hCDC group; at 28 days, *$P=0.01$ and **$P=0.004$ relative to the hCDC group. B, *$P<0.05$ relative to the hCDC group at 28 days.

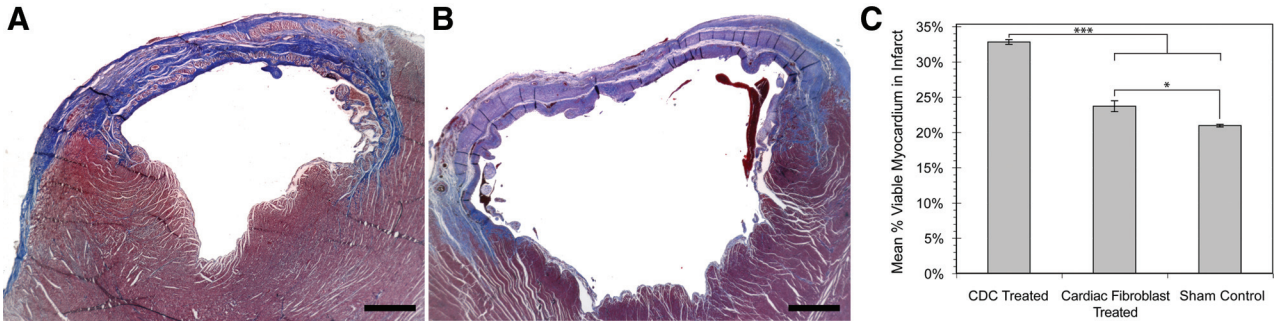


**Figure 8.** Quantification of regenerated myocardium was determined by Masson trichrome staining. A representative of the hCDCs transplanted into the infarcted myocardium (A) and media control (B). C, The calculated viable myocardium determined within the total infarct area of the hCDCs, fibroblast, and media control. *$P$=0.02 relative to cardiac fibroblast treated vs control; ***$P$<0.0001 relative to the hCDC group vs the cardiac fibroblast or control groups. The percentage of myocardium regenerated between the hCDC and control fibroblast groups was 9% and between the hCDC and control groups was 11.3%.

stained regions (viable tissue) within the predominately blue-stained (fibrous) infarct zone are evident in hearts transplanted with hCDCs. Fewer such regions were present with the cardiac fibroblast-treated hearts (Figure 8B). hCDC-transplanted hearts had a higher fraction of viable red-positive tissue (32.7±0.3%) within the infarct zone than the transplanted cardiac fibroblasts (24±0.7%; $P$<0.0001) or the control media–treated hearts (20±0.2%; $P$<0.0001; Figure 8C). We were able to quantify the myocardial regeneration attributable to hCDCs compared with that attributable to cardiac fibroblasts or control media. The increase in viable myocardium in hearts transplanted with hCDC was 1.4-fold and 1.8-fold greater than in hearts receiving cardiac fibroblasts or media, respectively.

## Discussion

To the best of our knowledge, this is the largest and first systematic investigation of the presence of progenitor cells in young, maturing, postnatal human myocardium. The major findings of our study are that resident hCDCs are present in the maturing postnatal human heart and are most abundant during the neonatal period. Regardless of age-dependent variations in resident hCPC numbers or congenital cardiac diagnoses, we demonstrated the validity of the cardiosphere method to reproducibly isolate and expand progenitor cells from RA tissues. In addition, we have shown the unique heterogeneity of cardiospheres with a spectrum of differentiated and undifferentiated cells, including ISL1- and c-kit–expressing cells. Finally, we showed that transplantation of hCDCs triggered myocardial regeneration and functional improvement after myocardial infarction.

### Comparison With Other Pediatric and Adult Studies

The first critical step toward clinical therapeutic application of autologous hCPCs in CHD patients is to anatomically locate resident hCPC populations within the young myocardium and to characterize their profile. Amir et al[18] examined resident hCPCs in right ventricular outflow tract tissue from young CHD patients and noticed a decline in c-kit$^+$ cells during the neonatal period. The samples were not taken from any other anatomic sites within the heart, and hCPCs were examined only during the neonatal period. Their study reported that c-kit$^+$ expression levels in human right ventricular outflow tract were significantly lower (≤1%) than what we report for RA (3% to 9%), suggesting that RA is a richer source of hCPCs; this has been confirmed separately by our finding of c-kit expression within the heart. Furthermore, Amir et al[18] performed no functional assays to determine the regenerative ability of the c-kit$^+$ cells. In adult human hearts, an initial study by Pouly et al[16] reported that the right-sided septum had higher c-kit$^+$ cells than the RA appendage in heart transplant patients who had varying degrees of active rejection. Recently, however, Itzhaki-Alfia[10] showed by multivariable linear regression analysis that more c-kit+ cells were isolated in adult human hearts in the RA than any other site within the heart, which corroborates our results from CHD patients. Furthermore, our findings are consistent with the distribution of resident hCPCs in the adult human heart, which is inversely correlated to regions sustaining the greatest hemodynamic load and wall stress.[13] This suggests increased accumulation of hCPCs in areas of reduced wall stress such as the RA.

Recently, a study by Anderson et al[19] raised the question of whether CDC populations and their novel characteristics were related to myofibroblastic contamination. In their study, CDC expression of CD90 and CD105 and production of collagen I were inferred as exclusive fibroblast markers, whereas the missing CDC expression of c-kit, ISL1, and NKX2–5 was presented as evidence of noncardiac progenitor status. A subsequent study by Davis et al[20] contradicted these findings, suggesting that experimental techniques may have altered the "CDC" population. Our present work corroborates the Davis et al publication and the majority of other cardiosphere studies.[6,8,11,21–24] We demonstrated expression of c-kit, NKX2–5, and ISL1 in intact cardiospheres and c-kit and NKX2–5 in our hCDCs.[20–22] Although we consistently observed CD90 and CD105 in hCDCs, these markers (also observed, for example, in adipose-derived progenitor cells) indicate only a mesenchymal phenotype and do not definitively identify fibroblasts.[24] Whereas Anderson et al noted a CD45$^+$ CDC subpopulation, our hCDCs were consistently negative for other Lin1 hematopoietic surface markers (CD3, CD14, CD16, CD19, CD20, and CD56). Finally, our hCDCs did not confirm the collagen I expression that Anderson et al

observed in their other CD45 collagen $1^+$ subpopulation (Figure V in the online-only Data Supplement).

### Implications for CHD Patients

We demonstrated that transplanted hCDCs derived from CHD patients have robust regenerative ability. Our data further support the strong regenerative ability of the young heart that is reflected by the higher percentage of stem cells indicated by elevated c-kit$^+$ expression in the neonates. A recent study reported similarly increased levels of c-kit$^+$ resident CPCs in neonatal mouse hearts and speculated that this phenomenon was associated with the greater cardiomyogenic differentiative potential of neonatal CPCs than adult-derived CPCs.[23] Although the mechanism(s) of cardiomyogenic differentiation by CPCs remain unclear, they may involve directed regeneration and/or paracrine effects. Our results would suggest that directed myocardial regeneration may play a key role in the functional improvement of the hCDC-transplanted hearts. A recent report suggests that adult cardiac resident progenitors elicit most of their beneficial effects by a paracrine mechanism.[24] Thus, it will be important to further determine the paracrine effects of hCDCs that serve to promote myocardial regeneration.

Although potentially broad areas of therapeutic utility for stem cell-based therapy in congenital heart patients include ischemic injuries, the vast majority of potential clinical applications would involve cardiomyopathy or congenital lesions. In patients with cardiac failure resulting from complex congenital heart disease, stem cell–based therapy may have promise as an alternative to transplantation. For instance, patients with single-ventricle lesions and severely depressed cardiac function have no long-term option other than transplantation. In this patient population, reversal of ventricular dysfunction with stem cell–based therapy has the potential to allow maintenance of the Fontan circulation. We also speculate that the delivery of stem cells to these single-ventricle lesion patients early in life at the time of their palliative surgeries may have the most beneficial improvement in their outcomes.

### Conclusions

Resident hCPCs are most abundant and proliferative during the neonatal period but decline rapidly with age. The RA is the most surgically accessible region in the hearts of young CHD patients and represents a uniquely rich source of endogenous hCPCs. The need for frequent surgical interventions in young CHD patients illustrates the utility of reserving RA tissue for hCDC harvest. We demonstrated the strong regenerative ability of hCDCs from CHD patients in an animal model of myocardial ischemia. Understanding the mechanisms regulating CDC differentiation after transplantation in nonischemic cardiomyopathic hearts is a prerequisite to the development of cell-based regenerative strategies for CHD.

## Acknowledgments

The helpful suggestions of Dr Doug Losordo are appreciated, and we thank Pat Heraty for her technical assistance.

## Sources of Funding

This work was supported by the following grants: National Institutes of Health (KO8HL097069), the Thoracic Surgical Foundation for Research and Education, the Children's Heart Foundation, and the North Suburban Medical Research Junior Board.

## Disclosures

None.

## References

1. Patel MS, Kogan BE. Care of the adult congenital heart disease patient in the United States: a summary of the current system. *Pediatr Cardiol.* 2010;31:511–514.
2. Kaushal S, Jacobs JP, Gossett JG, Steele A, Steele P, Davis CR, Pahl E, Vijayan K, Asante-Korang A, Boucek RJ, Backer CL, Wold LE. Innovation in basic science: stem cells and their role in the treatment of paediatric cardiac failure: opportunities and challenges. *Cardiol Young*. 2009;19(suppl 2):74–84.
3. Yi BA, Wernet O, Chien KR. Pregenerative medicine: developmental paradigms in the biology of cardiovascular regeneration. *J Clin Invest*. 2010;120:20–28.
4. Smith RR, Barile L, Messina E, Marbán E. Stem cells in the heart: what's the buzz all about, part 1: preclinical considerations. *Heart Rhythm*. 2008;5:749–757.
5. Dai W, Hale SL, Martin BJ, Kuang J-Q, Dow JS, Wold LE, Kloner RA. Allogenic mesenchymal stem cell transplantation in postinfarcted rat myocardium: short- and long-term effects. *Circulation*. 2005;112:214–223.
6. Smith RR, Barile L, Choo HC, Leppo MK, Hare JM, Messina E, Giacomello A, Abraham R, Marban E. Regenerative potential of cardiosphere derived cells expanded from percutaneous endomyocardial biopsy specimens. *Circulation*. 2007;115:896–908.
7. Urbanek K, Quaini F, Tasca G, Torella D, Castaldo C, Nadal-Ginard B, Leri A, Kajstura J, Quaini E, Anversa P. From the cover: intense myocyte formation from cardiac stem cells in human cardiac hypertrophy. *Proc Natl Acad Sci U S A*. 2003;100:10440–10445.
8. Messina E, De Angelis L, Frati G, Morrone S, Chimenti S, Fiordaliso F, Salio M, Battaglia M, Latronico MVG, Coletta M, Vivarelli E, Frati L, Cossu G, Giacomello A. Isolation and expansion of adult human cardiac stem cells from human and murine heart. *Circ Res*. 2004;95:911–921.
9. Bearzi C, Rota M, Hosoda T, Tillmanns J, Nascimbene A, De Angelis A, Yasuzawa-Amano S, Trofimova I, Siggins RW, LeCapitaine N, Cascapera S, Beltrami AP, D-Alessandro DA, Zias E, Quaini F, Urbanek K, Michler RE, Bolli R, Kajstura J, Leri A, Anversa P. Human cardiac stem cells. *Proc Natl Acad Sci U S A*. 2007;104:14068–14073.
10. Itzhaki-Alfia A, Leor J, Raanani E, Sternik L, Spiegelstein D, Netser S, Holbova R, Pevsner-Fischer M, Lavee J, Barbash IM. Patient characteristics and cell source determine the number of isolated human cardiac progenitor cells. *Circulation*. 2009;120:2559–2566.
11. Ott HC, Matthiesen TS, Brechtken J, Grindle S, Goh SK, Nelson W, Taylor DA. The adult human heart as a source for stem cells: repair strategies with embryonic-like progenitor cells. *Nat Clin Pract Cardiovasc Med*. 2007;4(suppl 1):S27–S39.
12. Simpson D, Liu H, Fan TH, Nerem R, Dudley SC Jr. A tissue engineering approach to progenitor cell delivery results in significant cell engraftment and improved myocardial remodeling. *Stem Cells*. 2007;25:2350–2357.
13. Leri A, Kajstura J, Anversa P. Cardiac stem cells and mechanisms of myocardial regeneration. *Physiol Rev*. 2005;85:1373–1416.
14. Durocher D, Charron F, Warren R, Schwartz RJ, Nemer M. The cardiac transcription factors Nkx2–5 and GATA-4 are mutual cofactors. *EMBO J*. 1997;16:5687–5696.
15. Nemir M, Pedrazzini T. Functional role of NOTCH signaling in the developing and postnatal heart. *J Mol Cell Card*. 2008;45:495–504.
16. Pouly J, Bruneval P, Mandet C, Proksh S, Peyard S, Amrein C, Bousseaux V, Guillemain R, Deloch A, Fabiani J, Menasche P. Cardiac stem cells in the real world. *J Thorac Cardiovasc Surg*. 2008;135:673–678.
17. Tateishi K, Ashihara E, Honsho S, Takehara N, Nomura T, Takahashi T, Ueyama T, Yamagishi M, Yaku H, Matsubara H, Oh H. Human cardiac stem cells exhibit mesenchymal features and are maintained through Akt/GSK-3B. *Biochem Biophys Res Commun*. 2007;352:635–641.

18. Amir G, Ma X, Reddy M, Hanley FL, Reinhartz O, Ramamoorthy C, Riemer RK. Dynamics of human myocardial progenitor cell populations in the neonatal period. *Ann Thorac Surg*. 2008;86:1311–1320.
19. Andersen DC, Andersen P, Schneider M, Jensen HB, Shiekh SP. Murine "cardiospheres" are not a source of stem cells with cardiomyogenic potential. *Stem Cells*. 2009;27:1571–1581.
20. Johnston PV, Sasano T, Mills K, Evers R, Lee ST, Smith RR, Lardo AC, Lai S, Steenbergen C, Gerstenblith G, Lange R, Marbán E. Engraftment, differentiation, and functional benefits of autologous cardiosphere-derived cells in porcine ischemic cardiomyopathy. *Circulation*. 2009;120:1075–1083.
21. Davis DR, Kizana E, Terrovitis J, Barth AS, Zhang Y, Smith RR, Miake J, Marbán E. Isolation and expansion of functionally-competent cardiac progenitor cells directly from heart biopsies, *J Mol Cell Cardiol*. 2010;49:312–321.
22. Davis DR, Ruckdeschel Smith R, Marban E. Human cardiospheres are a source of stem cells with cardiomyogenic potential. *Stem Cells*. 2010;28:903–904.
23. Zaruba M-M, Soonpaa M, Reuter S, Field LJ. Cardiomyogenic potential of C-Kit$^{+}$–expressing cells derived from neonatal and adult mouse hearts. *Circulation*. 2010;121:1992–2000.
24. Chimenti I, Smith R, Li T-S, Gerstenblith G, Messina E, Giacomello A, Marbán E. Relative roles of direct regeneration versus paracrine effects of human cardiosphere-derived cells transplanted into infarcted mice. *Circ Res*. 2010;106:971–980.

## CLINICAL PERSPECTIVE

Visionaries in the field of cardiac therapeutics have long looked to a future when damaged hearts could be rebuilt from the cellular level. Reports on bone marrow–derived stem cells and, more recently, endogenous cardiac progenitor cells have focused on their function and utility in rebuilding the hearts of adults. In the pediatric population, the majority of potential clinical applications would involve patients with cardiomyopathy or congenital lesions rather than adulthood ischemic injury. Our study investigated the presence of a resident pool of human cardiac progenitor cells and demonstrated how it changes during postnatal maturation in the nondiseased myocardium of young patients with congenital heart disease. We showed that resident human cardiac progenitor cells are present in the young myocardium and are most abundant during the neonatal period. Furthermore, these cells can be isolated from a wide range of congenital heart patients, including neonates and adolescents, as well as those with cyanosis. Our study suggests that the best source of human cardiac progenitor cells is the right atrium, from which small, clinically relevant myocardial specimens can be obtained. These isolated cells can be expanded in vitro and therefore provide a large number of cells for therapeutic applications. Our functional findings with these cells could enhance the development of novel cell-based regenerative approaches not yet explored in congenital heart patients.

# Characterization and Functionality of Cardiac Progenitor Cells in Congenital Heart Patients

Rachana Mishra, Kalpana Vijayan, Evan J. Colletti, Daniel A. Harrington, Thomas S. Matthiesen, David Simpson, Saik Kia Goh, Brandon L. Walker, Graça Almeida-Porada, Deli Wang, Carl L. Backer, Samuel C. Dudley, Jr, Loren E. Wold and Sunjay Kaushal

*Circulation.* 2011;123:364-373; originally published online January 17, 2011;
doi: 10.1161/CIRCULATIONAHA.110.971622
*Circulation* is published by the American Heart Association, 7272 Greenville Avenue, Dallas, TX 75231

Print ISSN: 0009-7322. Online ISSN: 1524-4539

# Correction

In the article by Mishra et al. "Characterization and Functionality of Cardiac Progenitor Cells in Congenital Heart Patients," which published in the February 1, 2011 issue of the journal (*Circulation*. 2011;123:364–373), the senior author of Reference 18 is incorrectly listed as "Reimer KR." The correct name is "Riemer RK."

The correction has been made in the current online version of the article. The authors regret the error.

**DOI: 10.1161/CIR.0b013e31823f916c**

**(*Circulation*. 2012;124:e958.)**


***Circulation* is available at http://circ.ahajournals.org**

# Expanded Methods For Mishra et al, "CHARACTERIZATION AND FUNCTIONALITY OF CARDIAC PROGENITOR CELLS IN CONGENITAL HEART PATIENTS

*Tissue fixation and histological processing*

Heart samples obtained were immersed in ice cold PBS. Thin strips of tissue were pinned slightly stretched and submerged in ice-cold PBS containing 4% paraformaldehyde for 1 hour. Tissues were then cut into 5 mm cubes and incubated in fresh fixative for 1 hour. After several PBS washes, tissues were cryoprotected in PBS containing increasing sucrose concentrations, ranging from 5% to 20%. Tissues were then incubated in 2 parts 20% sucrose, 1 part OCT compound (TissueTek) for 1 hour and embedded in fresh solution by rapid freezing in isopentane cooled in liquid nitrogen. A Leica microtome was used to section each tissue and cryosections 7 to 10 μm thick, were adhered to Fisherbrand Superfrost/Plus microscope slides.

Tissue sections were washed with PBS, and blocked in PBS containing 10% normal goat serum (NGS) or 2% bovine serum albumin (BSA). Sections were then incubated in PBS with 2% NGS or 0.5% BSA and diluted primary antibody overnight at 4°C. Slides were washed with PBS with 2% NGS or 0.5% BSA and then incubated with secondary antibody in PBS with 2% NGS or 0.5% BSA for 1 hour at 4°C. Finally, tissue sections were counterstained with DAPI (Biogenex) and sealed with Cytoseal 60 (Richard-Allen Scientific). An Olympus Fluoview 1000 confocal microscope system was used to visualize and capture images of antibody mediated immunofluorescence. Primary antibodies used were c-kit (Abcam, ab60585 & ab5506), Ki67 (Thermo Scientific, RB-1510-p1), Nkx2.5 (R&D, mab2444), Troponin 1 (TnI) (Abcam, ab47003), Smooth Muscle Actin (Sigma, SAB250), CD31/PECAM (R&D Systems Inc., BBA7), Troponin I (ThermoFisher, MS29500), Human Nucleus Marker (Milipore. MAB1281), Sacromeric alpha actin (Sigma, A2172), Connexin 43 (Sigma, C6219), and von Willebrand (Sigma, HPA00185).

*Immunostaining of Cardiospheres*

Cardiospheres were collected when they had reached 100 to 1000 cells in size. Cardiospheres were frozen in OCT and sectioned at 5μm slices. Cardiosphere sections were fixed in ice cold acetone for 10 min. the slides were blocked with 10% normal goat serum for 45 min in room temperature. Slides were sequentially incubated with diluted primary and secondary antibody for 1 hour in room temperature. Between each step, slides were washed three times (1-5 min each) with 0.1% BSA/PBS. We used primary antibodies against c-kit (H-300, Santa Cruz Biotechnology), GATA-4 (56-327, BD Biosciences), cardiac tropinin I (ab52862, abscam), Isl-1 (R&D Systems, AF1837) and Nkx2.5 (MAB2444, R&D Systems Inc.). For secondary antibodies conjugated, AlexaFluor fluorochromes

were used (Invitrogen). Slides were counterstained with DAPI, and imaged by epifluorescence micrscopy (Leica DM-IRB inverted microscope).

*Immunostaining of CDC*

CDC on chamber slides were washed with PBS and fixed with 4% paraformaldehyde for 10 minutes. The cells were then permeabilized with 0.01% triton-X 100 for 3 minutes.

Prior to immunostaining, cells were blocked with PBS containing 3% BSA. Cells were incubated with primary antibodies to α-sacromeric actin (Abcam cat#ab7799), collagen I (Millipore, cat#MAB3391), connexin 43 (CS43) (Chemicon ca#MAB3067), Myosin heavy chain (MHC) R&D Systems ca# MAB4470), Sacroplasmic reticulum $Ca^{2+}$ ATPase (SERCA2) (Novus Biologicals cat#NB100-237), CD105 (R&D Systems cat# MAB10972), CD90 (BD Biosciences cat#555593), c-kit (R&D systems cat# AF332), Nkx2.5 R&D Systems cat#MAB2444), SSEA-4 (R&D Systems cat#MAB1435) and Oct3/4 (R&D Systems cat#MAB1759). After subsequent incubation with fluorescence tagged secondary antibodies cells were treated with DAPI (1mg/ml). The slides were mounted in Prolong™ (Invitrogen) and visualized by confocal microscopy (Zeiss 510 META).

*Flow Cytometry analysis of CDC*

c-kit (BD Biosciences cat#550412) CD90 (R&D Systems cat#FAB2067A & FAB2067P), CD105 (R&D Systems cat#FAB10971P) and a lineage cocktail (Lin1) (BD Biosciences cat#34056) of antibodies against hematopoietic lineage surface markers CD3, CD14, CD16, CD19, CD20, and CD56 were used. Labeled cells were analyzed on a Becton-Dickenson FACS Calibur with 10,000 events collected.

*In Vitro* Cardiac Lineage Differentiation Assays

For cardiomyocyte differentiation, cells were plated at 30,000 cells/$cm^2$ and treated with 10umol/L of 5-azacytidine in DMEM containing 10% FBS for 24 hours. The cells were then maintained in 2% FBS without 5-azacytidine for 2 weeks and then stained for cardiac troponin I and sarcomeric actin for assessment of differentiation. For endothelial cell differentiation, cells were plated at 30,000 cells/$cm^2$ and treated with 10 ng/ml vascular endothelial growth factor 165 (R&D Systems) in DMEM containing 10% FBS for 14 days with fractional medium change every 2 days and stained for von Willebrand factor (vWF) and CD31 for assessment of endothelial differentiation. For smooth muscle cell differentiation, cells were plated at lower density (3000 cells/$cm^2$) and treated with 5 ng/ml platelet-derived growth factor-BB, 2.5 ng/ml human transforming growth factor β1(R&D Systems) in DMEM containing 10% FBS for 14 days, with fractional medium changes of 50% every 2 days. Cells were stained for smooth muscle actin to determine smooth muscle differentiation.

Cell Transplantation and Echocardiography

Briefly, the rats were anesthetized with 1.5% isoflurane, intubated, and ventilated. A left thoracotomy was performed, the LAD was ligated, and after ten minutes, either cell ($1x10^6$) or media (roughly 300□l) were injected into four to five regions within the infarct and peri-infarct regions. The hCDCs were from patients (n=6) who were between 2 months and 6 months of age. Rats were allowed to recover under close supervision and supplemented with analgesics.

Transthoracic echocardiograms were performed on the rats using a Visual Sonics Vevo 770 series 17.5-MHz transducer. The rats were lightly anesthesized with 1% isoflurane and temperature maintained at 37ºC. Animal heart rate was maintained above 300 beats per
minute for the duration of the examination. Two-dimensional and M-mode echocardiography were used to assess wall motion, chamber dimensions, fractional shortening, and ejection fraction, while color flow Doppler was used to determine valve function. Baseline echocardiograms were acquired before LAD ligation with additional echocardiograms acquired at 7 days and 28 days after infarction. The images were obtained in triplicate by an echocardiographer who was blinded to the treatment group.

## ***Figure Captions***

**Figure SI-1**
Quantification of c-kit expression in the four different chambers of the heart by confocal microscopy. *** $P<0.05$

**Figure S1-2**
Confocal microscopy images identify c-kit$^+$tryptase$^+$ co-expression (a-c) which occurred at very low rate (<0.5%). Tryptase expression and c-kit expression are shown with DAPI staining in (a) and (b) repectively while co-expression is shown in (c).

**Figure SI-3**
Growth profiles for hCDCs are shown (a-c). Graph (a) shows growth over time of 3 different hCDC harvest generations (1, 2, 3) from 2 separate patient RA specimens. Graphs (b) and (c) compare growth of hCDC harvest generations 2 and 3 from multiple patient RA specimens. Patient ages indicated in legend.

**Figure SI-4**
Confocal microscopy images of CDC at early passage (P0) are shown. CDC expressing SSEA-4 and Oct3/4 are shown (a & b). Both SSEA-4 and Oct3/4 expression were rare and inconsistent between CDC across different patient samples. C-kit expression is shown in (c). The majority of CDC at P0 expressed Nkx2.5 (d).

**Figure SI-5**
Confocal microscopy images identify no fibroblast cells within the CDCs while the human fibroblasts were used as the positive control. Collagen type I was used as the positive marker for smooth muscle cells and DAPI identified the nuclei in blue.

Table S1

| < 30 Days | 1 month – ≤ 2 years | > 2 years – ≤ 13 years |
|---|---|---|
| *Transposition of the Great Arteries (6) | Ventricular Septal Defect (19) | Anomalous Aortic Origin of Coronary Artery (8) |
| *Hypoplastic Left Heart Syndrome (4) | *Tetralogy of Fallot (8) | Secundum Atrial Septal Defect (4) |
| *Total Anomalous Pulmonary Venous Connection (4) | Atrioventricular Septal Defect (6) | Aortic Stenosis, Valvar (2) |
| *Pulmonary Atresia (3) | Aortic Stenosis, Subvalvar (2) | Aortic Stenosis, Subvalvar (2) |
| Coarctation of Aorta (2) | Secundum Atrial Septal Defect (2) | Atrioventricular Septal Defect (2) |
| Interrupted Aortic Arch (2) | Vascular Ring (2) | Coarctation of Aorta (2) |
| *Tetralogy of Fallot (2) | Cor Triatriatum (1) | Aortic Aneurysm (1) |
| Truncus Arteriosus (2) | *Double Chambered Right Ventricle (1) | Cardiomyopathy (1) |
| Aortopulmonary Window (1) | Double Outlet Right Ventricle (1) | Double Inlet Left Ventricle (1) |
| Atrioventricular Septal Defect (1) | Heterotaxy (1) | Double Outlet Right Ventricle (1) |
| | Partial Anomalous Pulmonary Venous Connection (1) | Congenitally Corrected Transposition of the Great Arteries (1) |
| | *Pulmonary Atresia (1) | *Pulmonary Atresia (1) |
| | Tracheal Stenosis (1) | *Pulmonary Venous Stenosis (1) |
| | *Tricuspid Atresia (1) | Transposition of the Great Arteries (1) |
| | | Ventricular Septal Defect (1) |

*Cyanotic lesion

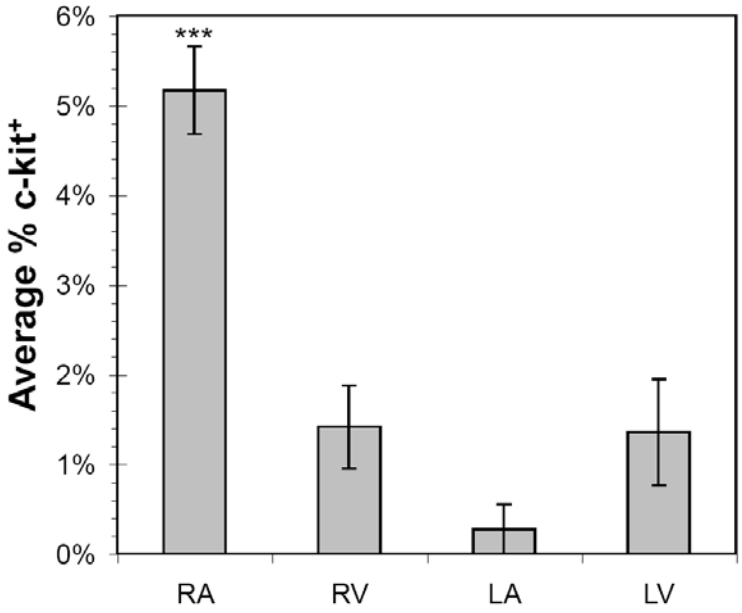


Figure. S1-1

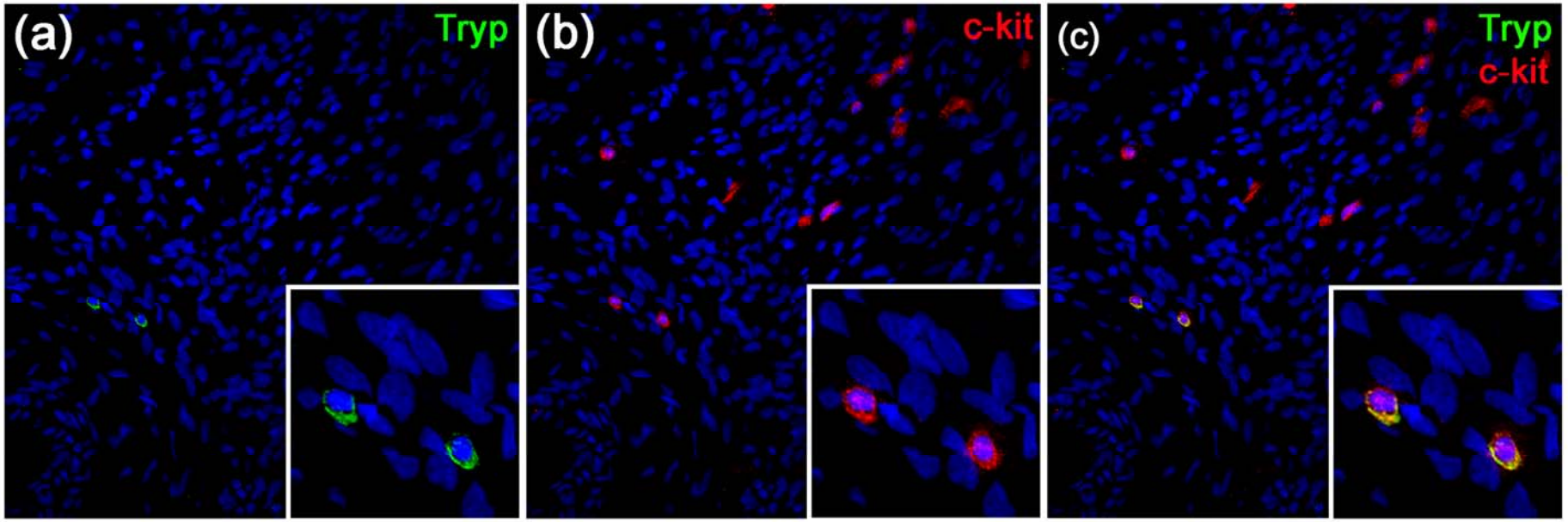


Figure S1-2

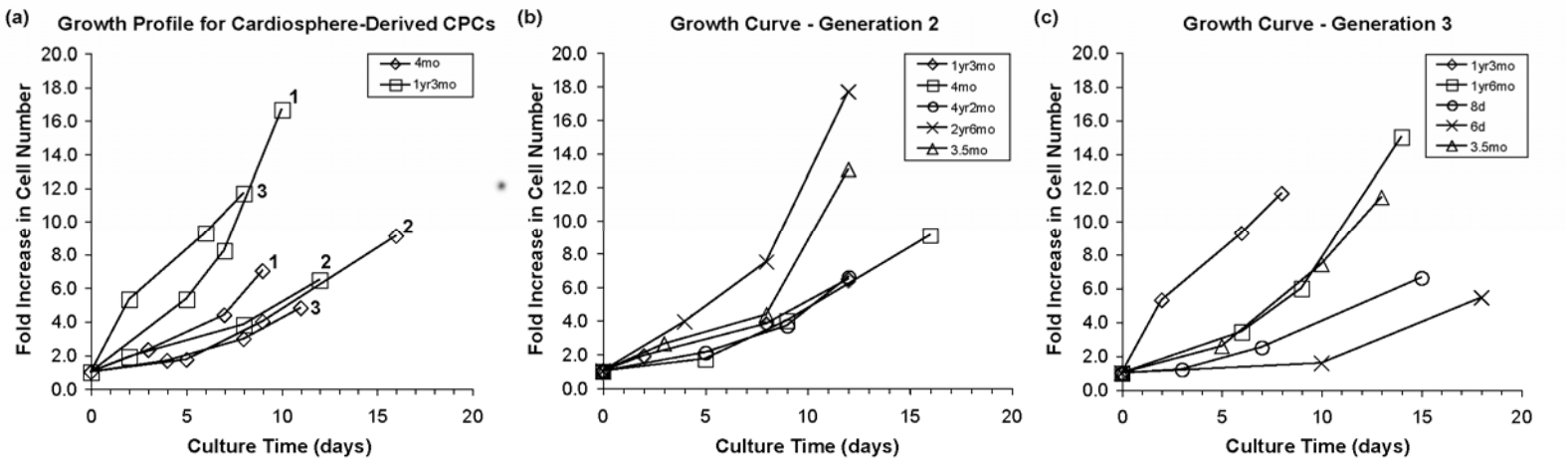
(a)
Growth Profile for Cardiosphere-Derived CPCs
Fold Increase in Cell Number
Culture Time (days)
4mo
1yr3mo
(b)
Growth Curve - Generation 2
Fold Increase in Cell Number
Culture Time (days)
1yr3mo
4mo
4yr2mo
2yr6mo
3.5mo
(c)
Growth Curve - Generation 3
Fold Increase in Cell Number
Culture Time (days)
1yr3mo
1yr6mo
8d
6d
3.5mo

Figure S1-3

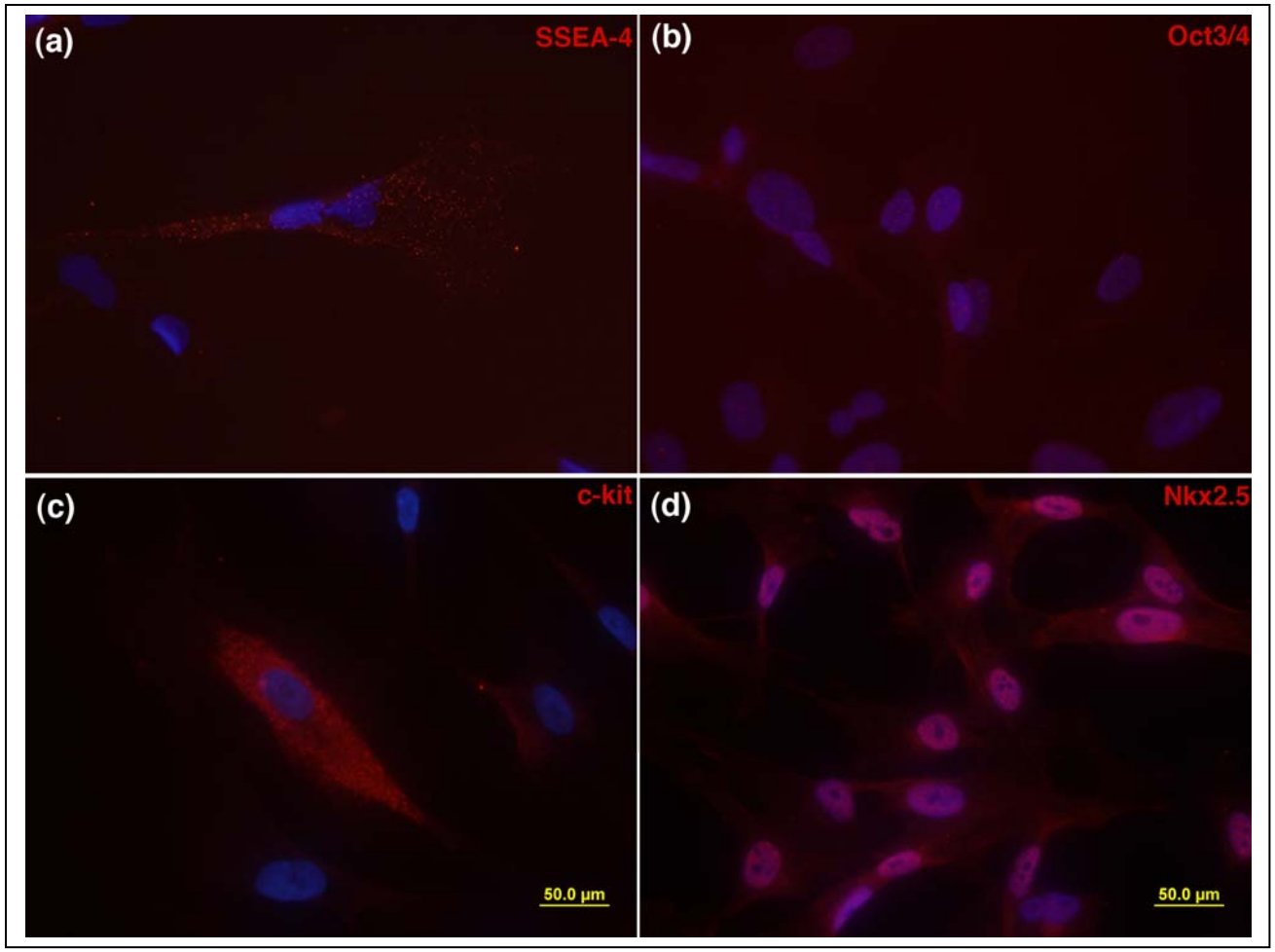


Figure S1-4

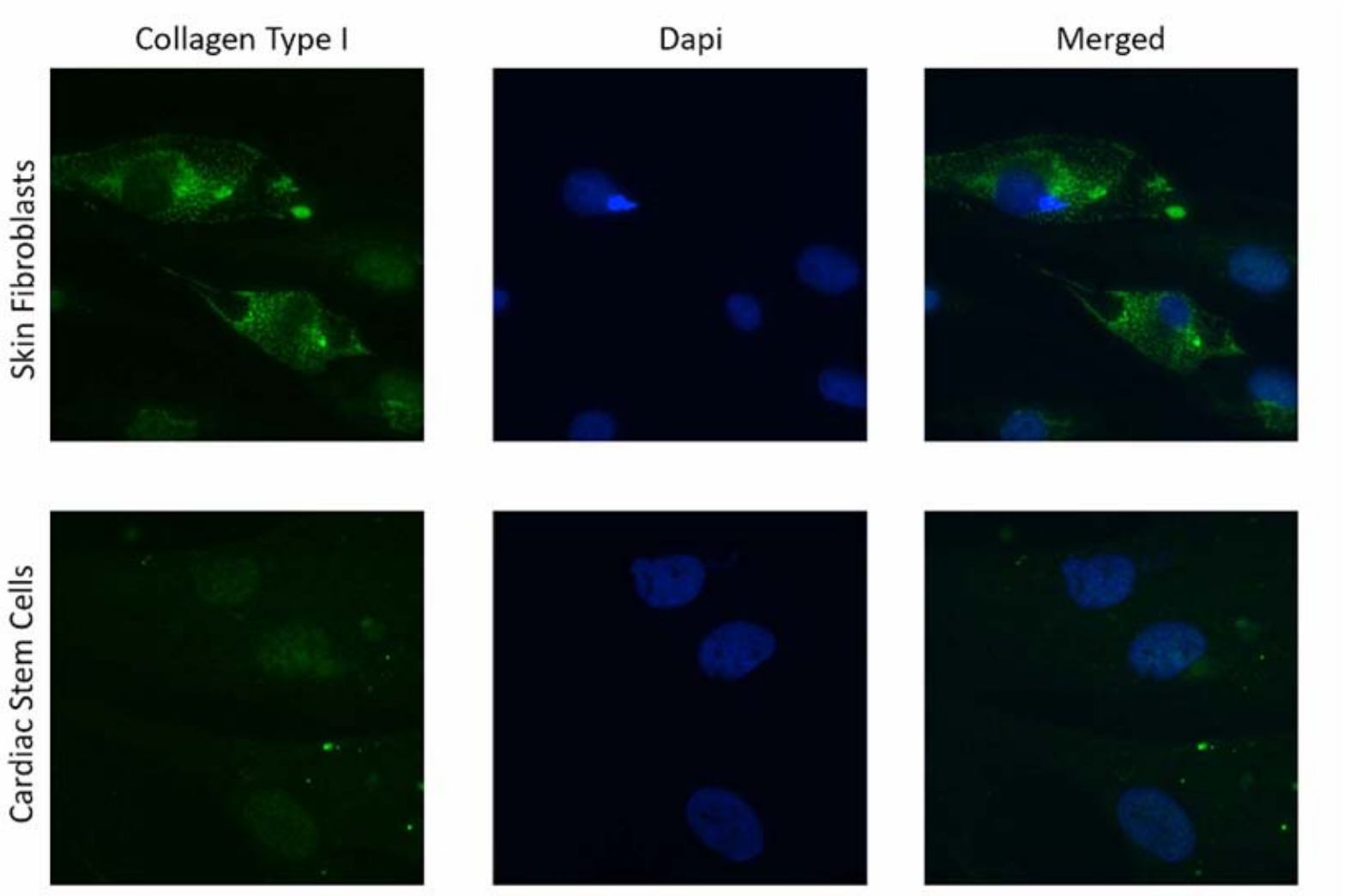
Collagen Type I
Dapi
Merged
Skin Fibroblasts
Cardiac Stem Cells

Figure S1-5

# Expanded Methods For Mishra et al, "CHARACTERIZATION AND FUNCTIONALITY OF CARDIAC PROGENITOR CELLS IN CONGENITAL HEART PATIENTS

*Tissue fixation and histological processing*

Heart samples obtained were immersed in ice cold PBS. Thin strips of tissue were pinned slightly stretched and submerged in ice-cold PBS containing 4% paraformaldehyde for 1 hour. Tissues were then cut into 5 mm cubes and incubated in fresh fixative for 1 hour. After several PBS washes, tissues were cryoprotected in PBS containing increasing sucrose concentrations, ranging from 5% to 20%. Tissues were then incubated in 2 parts 20% sucrose, 1 part OCT compound (TissueTek) for 1 hour and embedded in fresh solution by rapid freezing in isopentane cooled in liquid nitrogen. A Leica microtome was used to section each tissue and cryosections 7 to 10 μm thick, were adhered to Fisherbrand Superfrost/Plus microscope slides.

Tissue sections were washed with PBS, and blocked in PBS containing 10% normal goat serum (NGS) or 2% bovine serum albumin (BSA). Sections were then incubated in PBS with 2% NGS or 0.5% BSA and diluted primary antibody overnight at 4°C. Slides were washed with PBS with 2% NGS or 0.5% BSA and then incubated with secondary antibody in PBS with 2% NGS or 0.5% BSA for 1 hour at 4°C. Finally, tissue sections were counterstained with DAPI (Biogenex) and sealed with Cytoseal 60 (Richard-Allen Scientific). An Olympus Fluoview 1000 confocal microscope system was used to visualize and capture images of antibody mediated immunofluorescence. Primary antibodies used were c-kit (Abcam, ab60585 & ab5506), Ki67 (Thermo Scientific, RB-1510-p1), Nkx2.5 (R&D, mab2444), Troponin 1 (TnI) (Abcam, ab47003), Smooth Muscle Actin (Sigma, SAB250), CD31/PECAM (R&D Systems Inc., BBA7), Troponin I (ThermoFisher, MS29500), Human Nucleus Marker (Milipore. MAB1281), Sacromeric alpha actin (Sigma, A2172), Connexin 43 (Sigma, C6219), and von Willebrand (Sigma, HPA00185).

*Immunostaining of Cardiospheres*

Cardiospheres were collected when they had reached 100 to 1000 cells in size. Cardiospheres were frozen in OCT and sectioned at 5μm slices. Cardiosphere sections were fixed in ice cold acetone for 10 min. the slides were blocked with 10% normal goat serum for 45 min in room temperature. Slides were sequentially incubated with diluted primary and secondary antibody for 1 hour in room temperature. Between each step, slides were washed three times (1-5 min each) with 0.1% BSA/PBS. We used primary antibodies against c-kit (H-300, Santa Cruz Biotechnology), GATA-4 (56-327, BD Biosciences), cardiac tropinin I (ab52862, abscam), Isl-1 (R&D Systems, AF1837) and Nkx2.5 (MAB2444, R&D Systems Inc.). For secondary antibodies conjugated, AlexaFluor fluorochromes

were used (Invitrogen). Slides were counterstained with DAPI, and imaged by epifluorescence micrscopy (Leica DM-IRB inverted microscope).

*Immunostaining of CDC*

CDC on chamber slides were washed with PBS and fixed with 4% paraformaldehyde for 10 minutes. The cells were then permeabilized with 0.01% triton-X 100 for 3 minutes.

Prior to immunostaining, cells were blocked with PBS containing 3% BSA. Cells were incubated with primary antibodies to α-sacromeric actin (Abcam cat#ab7799), collagen I (Millipore, cat#MAB3391), connexin 43 (CS43) (Chemicon ca#MAB3067), Myosin heavy chain (MHC) R&D Systems ca# MAB4470), Sacroplasmic reticulum $Ca^{2+}$ ATPase (SERCA2) (Novus Biologicals cat#NB100-237), CD105 (R&D Systems cat# MAB10972), CD90 (BD Biosciences cat#555593), c-kit (R&D systems cat# AF332), Nkx2.5 R&D Systems cat#MAB2444), SSEA-4 (R&D Systems cat#MAB1435) and Oct3/4 (R&D Systems cat#MAB1759). After subsequent incubation with fluorescence tagged secondary antibodies cells were treated with DAPI (1mg/ml). The slides were mounted in Prolong™ (Invitrogen) and visualized by confocal microscopy (Zeiss 510 META).

*Flow Cytometry analysis of CDC*

c-kit (BD Biosciences cat#550412) CD90 (R&D Systems cat#FAB2067A & FAB2067P), CD105 (R&D Systems cat#FAB10971P) and a lineage cocktail (Lin1) (BD Biosciences cat#34056) of antibodies against hematopoietic lineage surface markers CD3, CD14, CD16, CD19, CD20, and CD56 were used. Labeled cells were analyzed on a Becton-Dickenson FACS Calibur with 10,000 events collected.

*In Vitro* Cardiac Lineage Differentiation Assays

For cardiomyocyte differentiation, cells were plated at 30,000 cells/$cm^2$ and treated with 10umol/L of 5-azacytidine in DMEM containing 10% FBS for 24 hours. The cells were then maintained in 2% FBS without 5-azacytidine for 2 weeks and then stained for cardiac troponin I and sarcomeric actin for assessment of differentiation. For endothelial cell differentiation, cells were plated at 30,000 cells/$cm^2$ and treated with 10 ng/ml vascular endothelial growth factor 165 (R&D Systems) in DMEM containing 10% FBS for 14 days with fractional medium change every 2 days and stained for von Willebrand factor (vWF) and CD31 for assessment of endothelial differentiation. For smooth muscle cell differentiation, cells were plated at lower density (3000 cells/$cm^2$) and treated with 5 ng/ml platelet-derived growth factor-BB, 2.5 ng/ml human transforming growth factor β1(R&D Systems) in DMEM containing 10% FBS for 14 days, with fractional medium changes of 50% every 2 days. Cells were stained for smooth muscle actin to determine smooth muscle differentiation.

Cell Transplantation and Echocardiography

Briefly, the rats were anesthetized with 1.5% isoflurane, intubated, and ventilated. A left thoracotomy was performed, the LAD was ligated, and after ten minutes, either cell ($1x10^6$) or media (roughly 300□l) were injected into four to five regions within the infarct and peri-infarct regions. The hCDCs were from patients (n=6) who were between 2 months and 6 months of age. Rats were allowed to recover under close supervision and supplemented with analgesics.

Transthoracic echocardiograms were performed on the rats using a Visual Sonics Vevo 770 series 17.5-MHz transducer. The rats were lightly anesthesized with 1% isoflurane and temperature maintained at 37ºC. Animal heart rate was maintained above 300 beats per
minute for the duration of the examination. Two-dimensional and M-mode echocardiography were used to assess wall motion, chamber dimensions, fractional shortening, and ejection fraction, while color flow Doppler was used to determine valve function. Baseline echocardiograms were acquired before LAD ligation with additional echocardiograms acquired at 7 days and 28 days after infarction. The images were obtained in triplicate by an echocardiographer who was blinded to the treatment group.

## ***Figure Captions***

**Figure SI-1**
Quantification of c-kit expression in the four different chambers of the heart by confocal microscopy. *** $P<0.05$

**Figure S1-2**
Confocal microscopy images identify c-kit$^+$tryptase$^+$ co-expression (a-c) which occurred at very low rate (<0.5%). Tryptase expression and c-kit expression are shown with DAPI staining in (a) and (b) repectively while co-expression is shown in (c).

**Figure SI-3**
Growth profiles for hCDCs are shown (a-c). Graph (a) shows growth over time of 3 different hCDC harvest generations (1, 2, 3) from 2 separate patient RA specimens. Graphs (b) and (c) compare growth of hCDC harvest generations 2 and 3 from multiple patient RA specimens. Patient ages indicated in legend.

**Figure SI-4**
Confocal microscopy images of CDC at early passage (P0) are shown. CDC expressing SSEA-4 and Oct3/4 are shown (a & b). Both SSEA-4 and Oct3/4 expression were rare and inconsistent between CDC across different patient samples. C-kit expression is shown in (c). The majority of CDC at P0 expressed Nkx2.5 (d).

**Figure SI-5**
Confocal microscopy images identify no fibroblast cells within the CDCs while the human fibroblasts were used as the positive control. Collagen type I was used as the positive marker for smooth muscle cells and DAPI identified the nuclei in blue.

Table S1

| < 30 Days | 1 month – ≤ 2 years | > 2 years – ≤ 13 years |
|---|---|---|
| *Transposition of the Great Arteries (6) | Ventricular Septal Defect (19) | Anomalous Aortic Origin of Coronary Artery (8) |
| *Hypoplastic Left Heart Syndrome (4) | *Tetralogy of Fallot (8) | Secundum Atrial Septal Defect (4) |
| *Total Anomalous Pulmonary Venous Connection (4) | Atrioventricular Septal Defect (6) | Aortic Stenosis, Valvar (2) |
| *Pulmonary Atresia (3) | Aortic Stenosis, Subvalvar (2) | Aortic Stenosis, Subvalvar (2) |
| Coarctation of Aorta (2) | Secundum Atrial Septal Defect (2) | Atrioventricular Septal Defect (2) |
| Interrupted Aortic Arch (2) | Vascular Ring (2) | Coarctation of Aorta (2) |
| *Tetralogy of Fallot (2) | Cor Triatriatum (1) | Aortic Aneurysm (1) |
| Truncus Arteriosus (2) | *Double Chambered Right Ventricle (1) | Cardiomyopathy (1) |
| Aortopulmonary Window (1) | Double Outlet Right Ventricle (1) | Double Inlet Left Ventricle (1) |
| Atrioventricular Septal Defect (1) | Heterotaxy (1) | Double Outlet Right Ventricle (1) |
| | Partial Anomalous Pulmonary Venous Connection (1) | Congenitally Corrected Transposition of the Great Arteries (1) |
| | *Pulmonary Atresia (1) | *Pulmonary Atresia (1) |
| | Tracheal Stenosis (1) | *Pulmonary Venous Stenosis (1) |
| | *Tricuspid Atresia (1) | Transposition of the Great Arteries (1) |
| | | Ventricular Septal Defect (1) |

*Cyanotic lesion

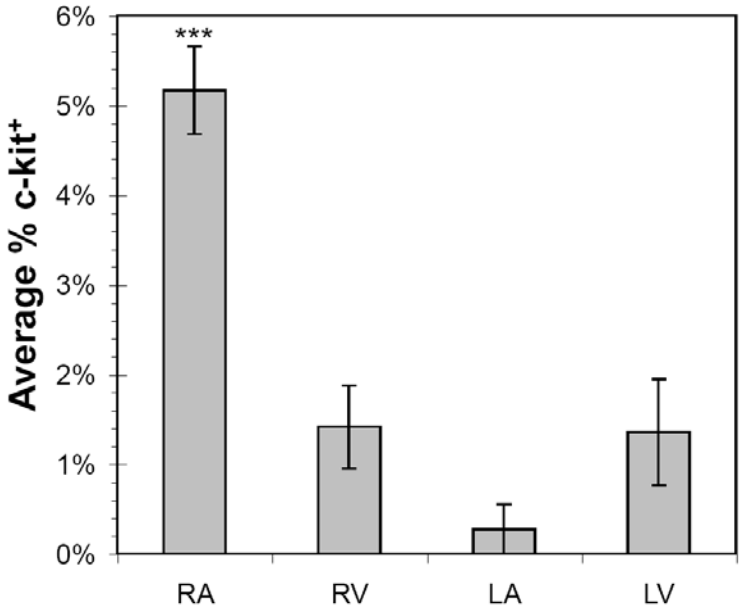


Figure. S1-1

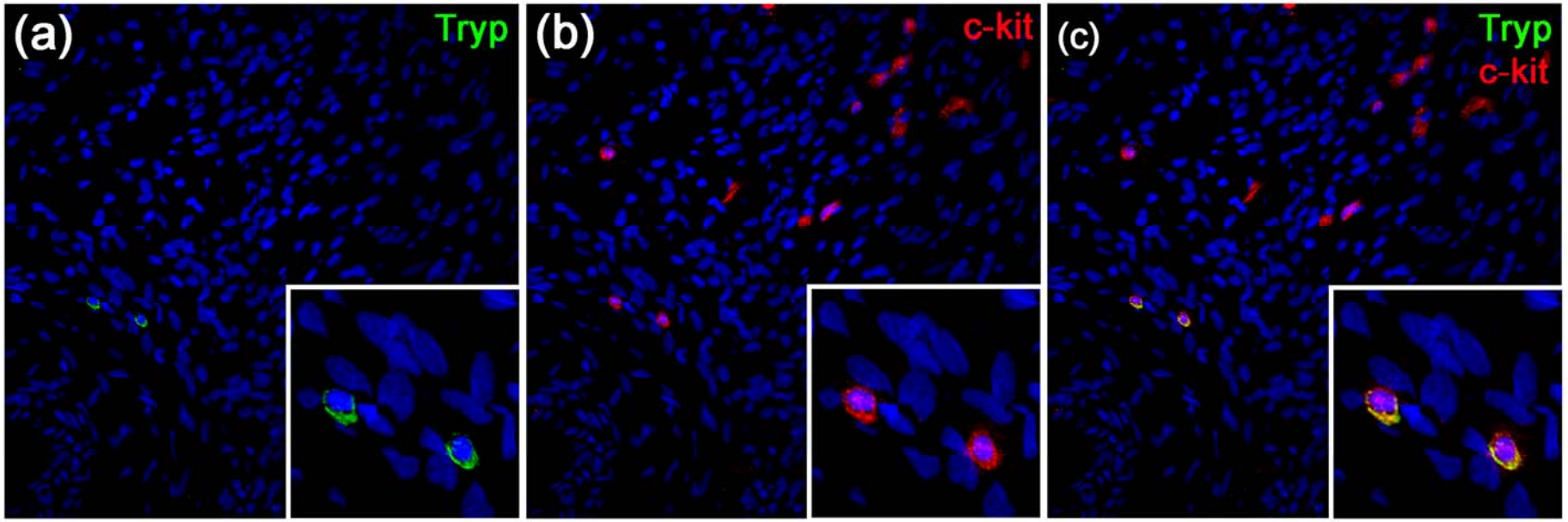


Figure S1-2

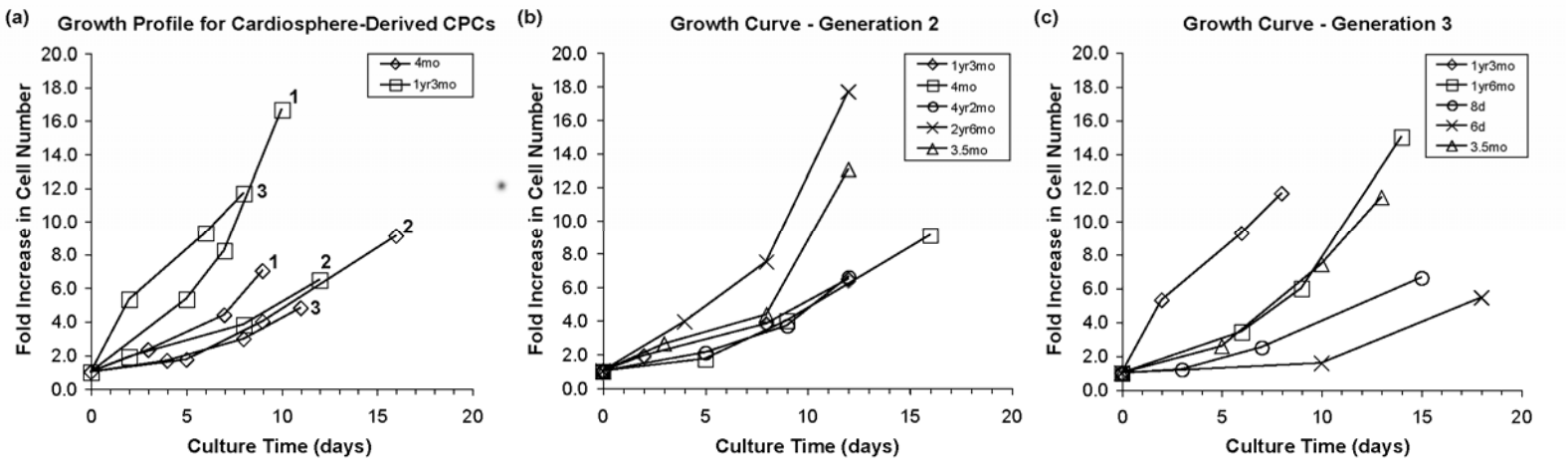
(a)
Growth Profile for Cardiosphere-Derived CPCs
Fold Increase in Cell Number
Culture Time (days)
4mo
1yr3mo
(b)
Growth Curve - Generation 2
Fold Increase in Cell Number
Culture Time (days)
1yr3mo
4mo
4yr2mo
2yr6mo
3.5mo
(c)
Growth Curve - Generation 3
Fold Increase in Cell Number
Culture Time (days)
1yr3mo
1yr6mo
8d
6d
3.5mo

Figure S1-3

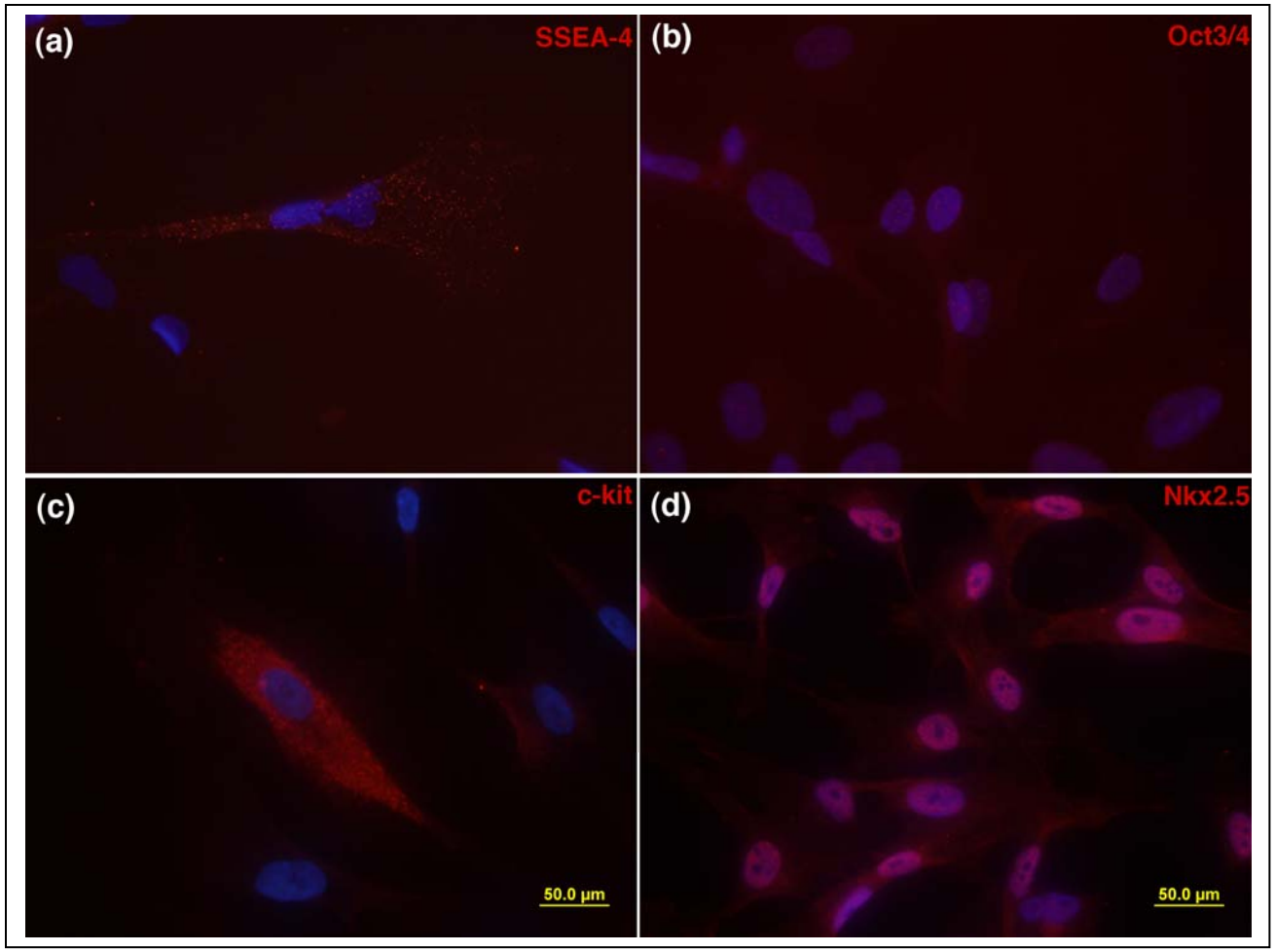


Figure S1-4

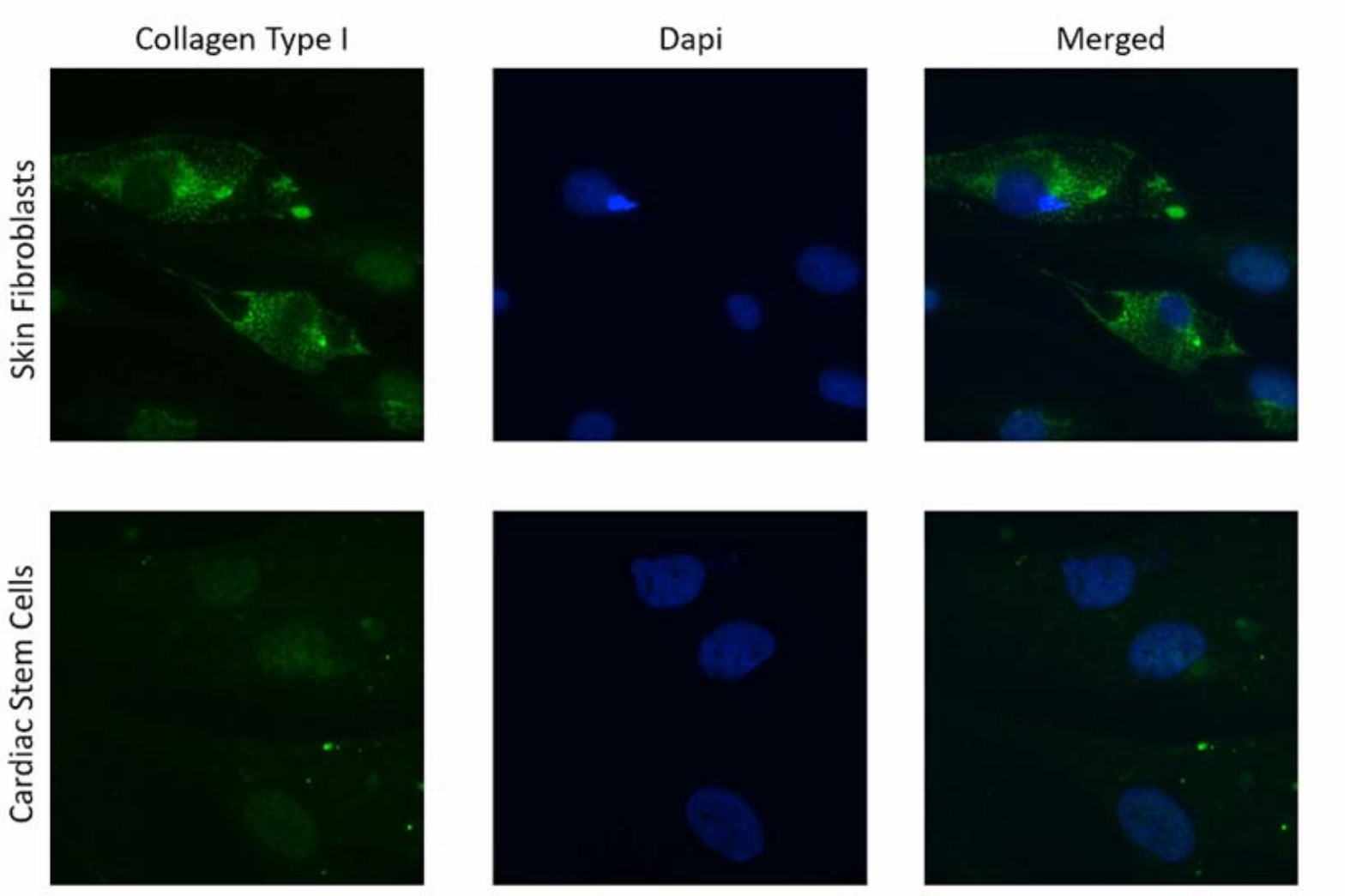
Collagen Type I
Dapi
Merged
Skin Fibroblasts
Cardiac Stem Cells

Figure S1-5